Modeling of Piezoelectric Devices With the Finite Volume Method

Valentin Bolborici, *Member, IEEE*, Francis P. Dawson, *Fellow, IEEE*, and Mary C. Pugh

***Abstract*—A partial differential equation (PDE) model for the dynamics of a thin piezoelectric plate in an electric field is presented. This PDE model is discretized via the finite volume method (FVM), resulting in a system of coupled ordinary differential equations. A static analysis and an eigenfrequency analysis are done with results compared with those provided by a commercial finite element (FEM) package. We find that fewer degrees of freedom are needed with the FVM model to reach a specified degree of accuracy. This suggests that the FVM model, which also has the advantage of an intuitive interpretation in terms of electrical circuits, may be a better choice in control situations.**

I. Introduction

Minimizing the size of electrical servo-drives used in small-scale actuation has become an important issue. Micro-satellites, micro-robot actuation, or servo-drives used in the automotive industry can exploit the properties of linear or rotary ultrasonic motors. These motors are actuators which are composed of piezoelectric materials. The piezoelectric materials can also be employed as sensors. When used as actuators, piezoelectric materials deliver force and/or displacement proportional to an applied voltage, and when used as sensors, they deliver a voltage proportional to the applied force. To use these devices as an actuator or as a sensor, one has to know how to model and control them properly.

The dynamics of a piezoelectric plate in an electric field can be modeled with a pair of coupled partial differential equations (PDE): a hyperbolic PDE for the displacements and Gauss' law for the electric displacement field. The finite element method (FEM) has been a popular choice for numerical studies of piezoelectric structures; some of the earlier works are [1]–[7]. One approach is to apply Hamilton's variational principle to the Lagrangian for the fully 3-D problem, which results in a variational structure within which one can use the FEM [1]. For piezoelectric materials that are thin in one direction, one can make approximations via a Taylor expansion in the thin direction, resulting in 2-D problems which can be studied with the FEM [3]. Also, for thin domains one can simply assume uniformity of the electric field and strain in the thin direction, resulting in a 2-D problem which fits into the variational formulation and can then be studied with the FEM [7]. The finite volume method (FVM), popular in various other areas of engineering, does not appear to have been applied to piezoelectric structures before.

In this paper, the finite volume method is used to discretize the PDE model, producing a system of ordinary differential equations (ODEs) whose solution approximates the solution of the PDE model. One can choose the discretization to meet a specified accuracy. Some reasons to consider the FVM discretization are:

- The FVM ODEs can be interpreted intuitively in terms of of equivalent electrical circuits of the piezoelectric system [8]. These circuits can then be implemented using schematic capture packages. This makes it easier to interface the FVM model of the piezoelectric system with the control circuits.
- In discretizing the PDE, one may have to make choices in how to apply the boundary conditions. As will be shown in Section V, the choices made in applying the boundary conditions can have significant impact on the rate of convergence of the discretized model to the true solution. The FVM approach allows one to implement these choices in a straightforward manner.
- The FVM works easily with surface integrals, making it easier to deal with phenomena that occur at the boundary between two different materials. Therefore, this method may be more suitable to model an ultrasonic motor because the operating principle of the motor is based on the friction mechanism that takes place at the common contact boundary between the stator and the rotor.

In this article, the FVM is applied to a thin piezoelectric plate, allowing the electric field to be assumed constant in space. Approximating the electric field in this way is common for thin piezoelectric materials and has the advantage of not only capturing the physics well but of also providing a simpler case study for numerical methods. Specifically, the system of coupled PDEs is reduced to a single PDE, resulting in a smaller system of ODEs after the discretization. However, the FVM could have equally well been applied to the full problem without this simplifying assumption.

II. The PDE Model

The constitutive equations for a linear piezoelectric material are

Manuscript received July 23, 2009; accepted March 20, 2010.

V. Bolborici and F. P. Dawson are with the Department of Electrical and Computer Engineering, University of Toronto, Toronto, ON, Canada (e-mail: valentin.bolborici@utoronto.ca).

M. C. Pugh is with the Department of Mathematics, University of Toronto, Toronto, ON, Canada.

Digital Object Identifier 10.1109/TUFFC.2010.1598

$$\mathbf{T} = \mathbf{c}^{\mathbf{E}}\mathbf{S} - \mathbf{e}^{t}\mathbf{E} \tag{1}$$

$$\mathbf{D} = \mathbf{e}\mathbf{S} + \varepsilon^{\mathbf{S}}\mathbf{E}. \tag{2}$$

The actuator equation (1) gives the stress, $\mathbf{T}(x, y, z, t)$, as a function of the strain, $\mathbf{S}(x, y, z, t)$, and the electric field, $\mathbf{E}(x, y, z, t)$, at each point in the material, at each moment in time. Similarly, the sensor equation (2) gives the charge density displacement vector, $\mathbf{D}(x, y, z, t)$, as a function of the strain and the electric field. The superscript t denotes the transpose and $\mathbf{c}^{\mathbf{E}}$ is the stiffness or elasticity matrix, $\varepsilon^{\mathbf{S}}$ is the dielectric matrix, and $\mathbf{e}$ is the electromechanical coupling term. The stiffness matrix, $\mathbf{c}^{\mathbf{E}}$, is evaluated at a constant electric field and the dielectric matrix, $\varepsilon^{\mathbf{S}}$, is evaluated at constant strain. From these, the dynamics of the piezoelectric material are determined [9] from Newton's second law

$$\rho \frac{\partial^2 \mathbf{u}}{\partial t^2} = \rho \mathbf{u}_{tt} = \nabla \cdot \mathbf{T}, \tag{3}$$

the absence of sources or sinks of charge

$$\nabla \cdot \mathbf{D} = \nabla \cdot \left(\mathbf{e}\mathbf{S} + \varepsilon^{\mathbf{S}}\mathbf{E} \right) = 0, \tag{4}$$

and appropriate boundary conditions. In (3), ρ is the mass density of the piezoelectric material and

$$\mathbf{u}(x, y, z, t) = \begin{pmatrix} u(x, y, z, t) \\ v(x, y, z, t) \\ w(x, y, z, t) \end{pmatrix}, \tag{5}$$

where u, v, and w are the local displacements from rest in the x, y, and z directions, respectively. At a point on the boundary of the material, one can specify either the displacements (u, v, and w) or the normal and tangential stresses.

Additional body forces can be modeled by including a body force density vector $\mathbf{K}(x, y, z)$ resulting in

$$\rho \mathbf{u}_{tt} = \nabla \cdot \mathbf{T} + \mathbf{K}. \tag{6}$$

Applying the finite volume method to this equation follows naturally [8] from the methods presented here for (3).

Eq. (3) does not contain any loss terms. Although in many applications it is understood that nonlinear hysteresis phenomena cannot be ignored, currently there is no known theory for incorporating mechanical and dielectric losses, starting from first principles, that account for nonlinear phenomena.

In this article, the piezoelectric material is assumed to be thin in the z direction (see Fig. 1) and so the approximation of a constant electric field is made. This approximation has been used in modeling of piezoelectric motors [7], [10], [11], piezoelectric transformers [12]–[14], and other piezoelectric actuators that use piezoelectric plates

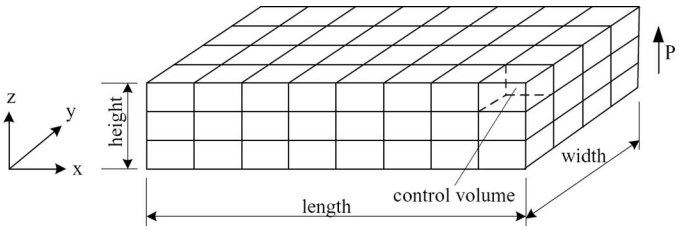

Fig. 1. Piezoelectric plate of height H, length L, and width W.

[15]–[17]. Specifically, rather than solving[1] equations (3) and (4) simultaneously for $\mathbf{u}$ and $\mathbf{E}$, the electric field $\mathbf{E}$ is assumed to be constant and in the z direction only:

$$\mathbf{E}(x, y, z, t) = \begin{pmatrix} 0 \\ 0 \\ E_3 \end{pmatrix}. \tag{7}$$

As a result, one only needs to solve (3) for $\mathbf{u}$. Once one has $\mathbf{u}$, the sensor equation (2) can then be used to determine the current withdrawn from the power supply at any moment in time. This, in turn, can be used to control the system.

III. The Finite Volume Method

The finite volume method (FVM) is generally used to obtain numerical solutions of conservation laws [18], [19]. Many behaviors in nature can be described via conservation laws such as conservation of mass, energy, or charge. A conservation law for a conserved quantity Φ can be written in the form:

$$\frac{\mathrm{d}\Phi}{\mathrm{d}t} = -\nabla \cdot \mathbf{F} + S. \tag{8}$$

That is, the rate of change of quantity Φ equals the divergence of the flux $\mathbf{F}$ plus any sources or sinks, S, of the quantity. Integrating the PDE (8) over a region Ω and applying the divergence theorem yields

$$\frac{\mathrm{d}}{\mathrm{d}t} \int_{\Omega} \Phi \mathrm{d}V = -\int_{\partial\Omega} \mathbf{F} \cdot \mathbf{n} \mathrm{d}A + \int_{\Omega} S \mathrm{d}V. \tag{9}$$

That is, the change in the amount of Φ in the region Ω is caused by the flux across the boundary, $\partial\Omega$, plus whatever sources and sinks occur within Ω. Here, $\mathbf{n}$ is the outward normal and $-\mathbf{F} \cdot \mathbf{n}$ corresponds to inward flow of Φ.

The finite volume method respects the conservation structure of the PDE—it keeps track of the fluxes at the boundary of each region, ensuring that the discretized version of Φ is conserved. In general, these ideas can be used

[1]The strain matrix, $\mathbf{S}$, is determined by derivatives of $\mathbf{u}$ and so the unknowns in (3)–(4) are $\mathbf{u}$ and $\mathbf{E}$.

for any PDE which has a divergence term in it, including the dynamic equation (3) for the piezoelectric material.

The basic steps in the finite volume method are:

1) Divide the computational domain into subdomains. This is known as grid generation.
2) Approximate the integrated PDE on each subdomain. This requires approximating the flux across the boundary of each subdomain. The process is also called discretization. This results in a system of equations for the unknowns

$$\Phi_i := \frac{1}{\mathrm{vol}(\Omega_i)} \int_{\Omega_i} \Phi \mathrm{d}\, V. \tag{10}$$

3) Solve the discretized system.

IV. Application of the Finite Volume Method to a Piezoelectric Plate

In the following, the dynamic equation (3) is considered for a piezoelectric plate (refer to Fig. 1). The plate is divided in a uniform manner so that all subdomains (called control volumes here) have the same size. Hence the accuracy of the approximate solution, which is linked to the size of the subdomains, is linked to the number of control volumes. The more control volumes there are, the more accurate is the approximate solution. In Section V, it is shown that it takes markedly fewer control volumes to approximate the displacements and natural frequencies of the piezoelectric plate using the FVM discretization than using COMSOL's FEM discretization (Comsol Inc., Burlington, MA).

A. Grid Generation

The piezoelectric plate is shown in Fig. 1. It is divided into $n_x n_y n_z$ control volumes each of length L/n_x, width W/n_y, and height H/n_z. If n_x, n_y, and n_z are all greater than 1, then each control volume is either an interior volume (has control volumes on all sides), a face volume (has one face in common with the boundary of the plate), an edge volume (has two faces in common), or a corner volume (has three faces in common). An interior control volume is shown in Fig. 2.

In approximating the fluxes across the faces of this interior control volume, one needs not only the six nearest neighbors (those that share a common face with this volume) but also the twelve next-nearest neighbors (those that share a common edge with this volume). The neighbors contained in the xz plane through the point P are shown in Fig. 3. Fig. 4 is the corresponding figure for the yz plane through the point P. Fig. 5 is the corresponding figure for the xy plane through the point P. Figs. 3–5 contain the distances between the center of the interior control volume, P, and neighboring control volumes as well as the distances between the centers of neighboring control volumes. When the piezoelectric plate is divided

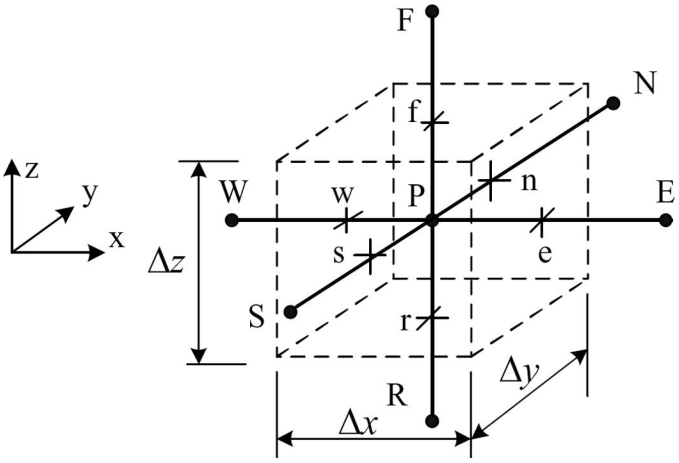

Fig. 2. An interior control volume. P labels its center. Its faces are labeled f (front), r (rear), e (east), w (west), n (north), and s (south). The centers of the corresponding nearest-neighbor control volumes are labeled E, W, N, S, F, and R.

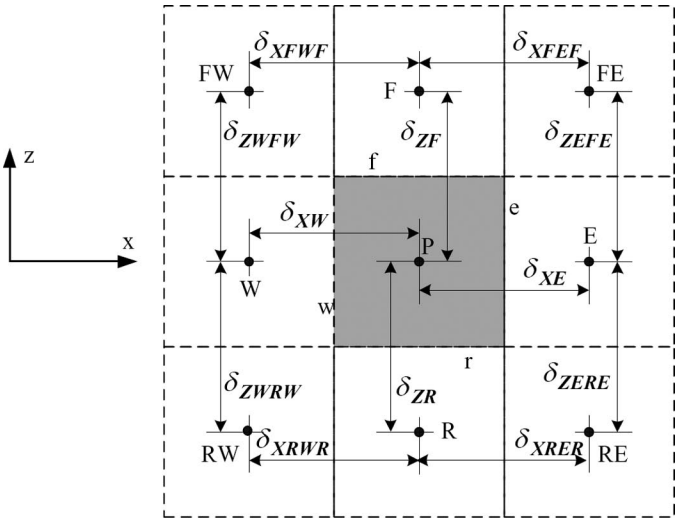

Fig. 3. An xz slice through the center of the interior control volume. The four faces appear as edges: f, e, r, and w. The nearest neighbors are as in Fig. 2. The four next-nearest neighbors have centers labeled FW, FE, RE, and RW. Some distances between different centers are also labeled.

in a uniform manner, these distances are one of L/n_x, W/n_y, or H/n_z. Fig. 6 gives the distances from P to the six faces of the control volume. In the subsequent FVM discretization, formulae are given referring to the distances given in Figs. 3–6, allowing for a non-uniform division of the piezoelectric plate.

B. Step 2: Discretization

Here, a set of ODEs is found to approximate the PDE (3). There are $3n_x n_y n_z$ ODEs, three for each control volume. The unknowns are $u_{ijk}(t)$, $v_{ijk}(t)$, and $w_{ijk}(t)$, which approximate the average value of the solution of (3) over the (i,j,k)th control volume:

$$\begin{pmatrix} u_{ijk}(t) \\ v_{ijk}(t) \\ w_{ijk}(t) \end{pmatrix} \approx \frac{1}{\mathrm{Vol}(V_{ijk})} \int_{V_{ijk}} \begin{pmatrix} u(x,y,z,t) \\ v(x,y,z,t) \\ w(x,y,z,t) \end{pmatrix} \mathrm{d}\, V. \tag{11}$$

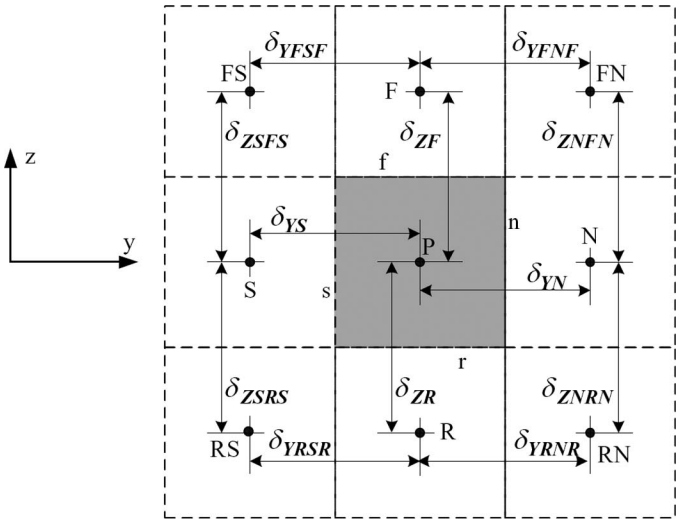

Fig. 4. A yz slice through the center of the interior control volume. The labeling is analogous to that given in Fig. 3.

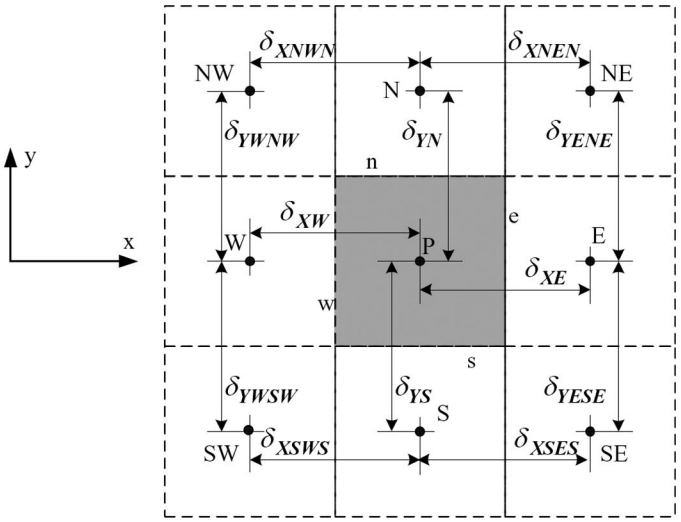

Fig. 5. An xy slice through the center of the interior control volume. The labeling is analogous to that given in Fig. 3.

In the following, rather than writing everything in terms of indices i, j, and k, the three ODEs are presented for a generic control volume centered at P.

Eq. (3) is integrated over the control volume ΔV shown in Fig. 7. This results in

$$\rho \frac{\mathrm{d}^2}{\mathrm{d}t^2} \int_{\Delta V} \begin{bmatrix} u \\ v \\ w \end{bmatrix} \mathrm{d}V = \int_{\Delta V} \nabla \cdot \begin{bmatrix} T_1 & T_6 & T_5 \\ T_6 & T_2 & T_4 \\ T_5 & T_4 & T_3 \end{bmatrix} \mathrm{d}V. \tag{12}$$

In (12), the symmetric stress tensor $\mathbf{T}$ is given in terms of six components $T_1, T_2, \ldots, T_6$. Applying the divergence theorem yields

$$\rho \frac{\mathrm{d}^2}{\mathrm{d}t^2} \int_{\Delta V} \begin{bmatrix} u \\ v \\ w \end{bmatrix} \mathrm{d}V = \int_{\partial \Delta V} \begin{bmatrix} T_1 & T_6 & T_5 \\ T_6 & T_2 & T_4 \\ T_5 & T_4 & T_3 \end{bmatrix} \mathbf{n} \mathrm{d}A. \tag{13}$$

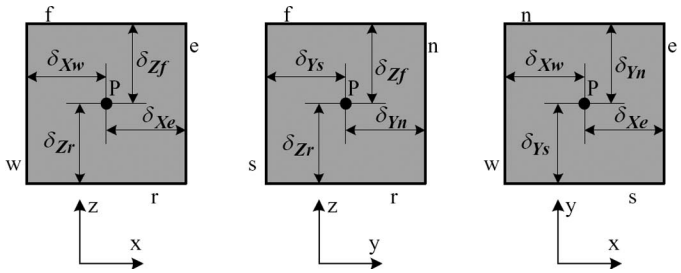

Fig. 6. Internal distances in the control volume of interest.

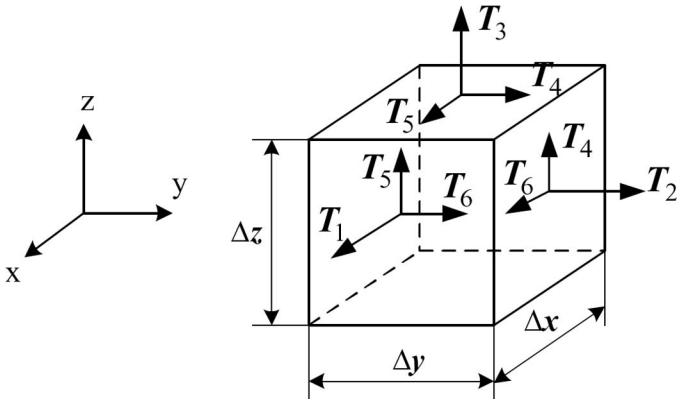

Fig. 7. The control volume ΔV and the stresses on its boundary. T_1, T_2, and T_3 are the normal stresses. T_4, T_5, and T_6 are the tangential stresses.

The surface integrals are calculated[2] on each of the bounding faces e, w, n, s, f, and r shown in Fig. 2. For example, the first component of (13) is

$$\rho \frac{\mathrm{d}^2}{\mathrm{d}t^2} \int_{\Delta V} u \mathrm{d}V = \int_{\mathrm{e}} T_1 \mathrm{d}y\mathrm{d}z - \int_{\mathrm{w}} T_1 \mathrm{d}y\mathrm{d}z + \int_{\mathrm{n}} T_6 \mathrm{d}x\mathrm{d}z - \int_{\mathrm{s}} T_6 \mathrm{d}x\mathrm{d}z + \int_{\mathrm{f}} T_5 \mathrm{d}x\mathrm{d}y - \int_{\mathrm{r}} T_5 \mathrm{d}x\mathrm{d}y. \tag{14}$$

The volume integral equals the average value of u in ΔV times the volume of ΔV and is denoted $u_{\mathrm{P}} \Delta x \Delta y \Delta z$. (As a convention, the average values of quantities in the control volume of interest will have the sub-index P. The average values in the neighboring elements will have the sub-indexes E, W, N, and so on.) Similarly, the surface integrals equal the average value over the corresponding face times the area of the face. For example, the first surface integral in (14) is denoted $T_{1e} \Delta y \Delta z$. Eq. (14) is then written as

[2]For the East face, e, the outward normal is $\mathbf{n} = (1\ 0\ 0)^t$. The differential area element is $\mathrm{d}y\mathrm{d}z$ and so the integral over this portion of the boundary $\partial \Delta V$ is

$$\int_{e} \begin{pmatrix} T_1 & T_6 & T_5 \\ T_6 & T_2 & T_4 \\ T_5 & T_4 & T_3 \end{pmatrix} \begin{pmatrix} 1 \\ 0 \\ 0 \end{pmatrix} \mathrm{d}y\mathrm{d}z = \int_{e} T_1 \mathrm{d}y\mathrm{d}z.$$

$$\rho\frac{\mathrm{d}^2u_{\mathrm{P}}}{\mathrm{d}t^2}\Delta x\Delta y\Delta z=(T_{1\mathrm{e}}-T_{1\mathrm{w}})\Delta y\Delta z+(T_{6\mathrm{n}}-T_{6\mathrm{s}})\Delta x\Delta z+(T_{5\mathrm{f}}-T_{5\mathrm{r}})\Delta x\Delta y. \tag{15}$$

This is an ODE for the average value of u in the control volume. However, one needs to write the stress tensor $\mathbf{T}$ in terms of the displacement $\mathbf{u}$. Like the stress tensor, the strain tensor $\mathbf{S}$ is symmetric and is determined by six components:

$$\mathbf{S}=\begin{bmatrix}S_1 & S_6 & S_5\\ S_6 & S_2 & S_4\\ S_5 & S_4 & S_3\end{bmatrix}, \tag{16}$$

The actuator and sensor equations (1) and (2) can then be written in a compact vector-matrix form:

$$\begin{bmatrix}T_1\\T_2\\T_3\\T_4\\T_5\\T_6\\D_1\\D_2\\D_3\end{bmatrix}=\begin{bmatrix}c_{11}&c_{12}&c_{13}&0&0&0\\c_{21}&c_{22}&c_{23}&0&0&0\\c_{31}&c_{32}&c_{33}&0&0&0\\0&0&0&c_{44}&0&0\\0&0&0&0&c_{55}&0\\0&0&0&0&0&c_{66}\\0&0&0&0&e_{15}&0\\0&0&0&e_{24}&0&0\\e_{31}&e_{32}&e_{33}&0&0&0\end{bmatrix}\begin{bmatrix}S_1\\S_2\\S_3\\S_4\\S_5\\S_6\end{bmatrix}-\begin{bmatrix}0&0&e_{31}\\0&0&e_{32}\\0&0&e_{33}\\0&e_{24}&0\\e_{15}&0&0\\0&0&0\\-\varepsilon_{11}&0&0\\0&-\varepsilon_{22}&0\\0&0&-\varepsilon_{33}\end{bmatrix}\begin{bmatrix}E_1\\E_2\\E_3\end{bmatrix} \tag{17}$$

The piezoelectric plate being modeled is thin in the z direction and has polarization oriented along the z axis. For this reason, the electric field is assumed to be constant and to be in the z direction ($E_1=E_2=0$).

In (15), the tensor components $T_{1\mathrm{e}}$, $T_{1\mathrm{w}}$, $T_{6\mathrm{n}}$, $T_{6\mathrm{s}}$, $T_{5\mathrm{f}}$, and $T_{5\mathrm{r}}$ are expressed as a function of the strains and the electric field, as shown in (17). The resulting equation is

$$\begin{aligned}\rho\frac{\mathrm{d}^2u_{\mathrm{P}}}{\mathrm{d}t^2}\Delta x\Delta y\Delta z&=(c_{11}S_{1\mathrm{e}}+c_{12}S_{2\mathrm{e}}+c_{13}S_{3\mathrm{e}}-e_{31}E_3)\Delta y\Delta z\\&\quad-(c_{11}S_{1\mathrm{w}}+c_{12}S_{2\mathrm{w}}+c_{13}S_{3\mathrm{w}}-e_{31}E_3)\Delta y\Delta z\\&\quad+c_{66}(S_{6\mathrm{n}}-S_{6\mathrm{s}})\Delta x\Delta z+c_{55}(S_{5\mathrm{f}}-S_{5\mathrm{r}})\Delta x\Delta y.\end{aligned} \tag{18}$$

In (18), the electric field component appears without subscripts e or w. This is because E_3 is assumed constant in space. As a result, its appearances in T_{1e} and T_{1w} cancel: the electric field does not enter in the ODEs for interior control volumes. The strain terms in (18) are now written as the derivatives of the displacements u, v, and w, as shown in [20]. Thus, (18) becomes

$$\begin{aligned}\rho\frac{\mathrm{d}^2u_{\mathrm{P}}}{\mathrm{d}t^2}\Delta x\Delta y\Delta z&=\left(c_{11}\frac{\partial u}{\partial x}\Big|_{\mathrm{e}}+c_{12}\frac{\partial v}{\partial y}\Big|_{\mathrm{e}}+c_{13}\frac{\partial w}{\partial z}\Big|_{\mathrm{e}}\right)\Delta y\Delta z\\&\quad-\left(c_{11}\frac{\partial u}{\partial x}\Big|_{\mathrm{w}}+c_{12}\frac{\partial v}{\partial y}\Big|_{\mathrm{w}}+c_{13}\frac{\partial w}{\partial z}\Big|_{\mathrm{w}}\right)\Delta y\Delta z\\&\quad+c_{66}\left(\frac{\partial u}{\partial y}\Big|_{\mathrm{n}}+\frac{\partial v}{\partial x}\Big|_{\mathrm{n}}-\frac{\partial u}{\partial y}\Big|_{\mathrm{s}}-\frac{\partial v}{\partial x}\Big|_{\mathrm{s}}\right)\Delta x\Delta z\\&\quad+c_{55}\left(\frac{\partial u}{\partial z}\Big|_{\mathrm{f}}+\frac{\partial w}{\partial x}\Big|_{\mathrm{f}}-\frac{\partial u}{\partial z}\Big|_{\mathrm{r}}-\frac{\partial w}{\partial x}\Big|_{\mathrm{r}}\right)\Delta x\Delta y.\end{aligned} \tag{19}$$

Eq. (19) holds exactly for any solution of the PDE (3); no approximations have been made. One now approximates the normal and tangential derivatives in (19). First, the case of an interior control volume is considered.

1) Interior Control Volumes: Such a control volume has control volumes on all sides and so the average value of a normal derivative over a face can be approximated by a linear function of the average displacements in the control volumes on either side of that face:

$$\frac{\partial u}{\partial x}\Big|_{\mathrm{e}}=\frac{u_{\mathrm{E}}-u_{\mathrm{P}}}{\delta_{\mathrm{XE}}}, \tag{20}$$

$$\frac{\partial u}{\partial x}\Big|_{\mathrm{w}}=\frac{u_{\mathrm{P}}-u_{\mathrm{W}}}{\delta_{\mathrm{XW}}}, \tag{21}$$

$$\frac{\partial u}{\partial y}\Big|_{\mathrm{n}}=\frac{u_{\mathrm{N}}-u_{\mathrm{P}}}{\delta_{\mathrm{YN}}}, \tag{22}$$

$$\frac{\partial u}{\partial y}\Big|_{\mathrm{s}}=\frac{u_{\mathrm{P}}-u_{\mathrm{S}}}{\delta_{\mathrm{YS}}}, \tag{23}$$

$$\frac{\partial u}{\partial z}\Big|_{\mathrm{f}}=\frac{u_{\mathrm{F}}-u_{\mathrm{P}}}{\delta_{\mathrm{ZF}}}, \tag{24}$$

$$\frac{\partial u}{\partial z}\Big|_{\mathrm{r}}=\frac{u_{\mathrm{P}}-u_{\mathrm{R}}}{\delta_{\mathrm{ZR}}}. \tag{25}$$

The tangential derivatives are approximated as follows. The average of the derivative $\partial v/\partial y$ over the East boundary is approximated by linear interpolation between the average of $\partial v/\partial y$ over the volume centered at P and the volume centered at E (refer to Figs. 5 and 6):

$$\frac{\partial v}{\partial y}\Big|_{\mathrm{e}}=\frac{\partial v}{\partial y}\Big|_{\mathrm{P}}\cdot\frac{\delta_{\mathrm{XE}}-\delta_{\mathrm{Xe}}}{\delta_{\mathrm{XE}}}+\frac{\partial v}{\partial y}\Big|_{\mathrm{E}}\cdot\frac{\delta_{\mathrm{Xe}}}{\delta_{\mathrm{XE}}}. \tag{26}$$

These, in turn, are approximated using the average displacements in the control volumes N, S, NE, and SE (refer to Fig. 5):

$$\frac{\partial v}{\partial y}\Big|_{\mathrm{P}}=\frac{v_{\mathrm{N}}-v_{\mathrm{S}}}{\delta_{\mathrm{YN}}+\delta_{\mathrm{YS}}}, \tag{27}$$

$$\left.\frac{\partial v}{\partial y}\right|_{\mathrm{E}} = \frac{v_{\mathrm{NE}} - v_{\mathrm{SE}}}{\delta_{\mathrm{YENE}} + \delta_{\mathrm{YESE}}}. \tag{28}$$

Substituting (27) and (28) into (26) yields:

$$\left.\frac{\partial v}{\partial y}\right|_{\mathrm{e}} = \frac{v_{\mathrm{N}} - v_{\mathrm{S}}}{\delta_{\mathrm{YN}} + \delta_{\mathrm{YS}}} \cdot \frac{\delta_{\mathrm{XE}} - \delta_{\mathrm{Xe}}}{\delta_{\mathrm{XE}}} + \frac{v_{\mathrm{NE}} - v_{\mathrm{SE}}}{\delta_{\mathrm{YENE}} + \delta_{\mathrm{YESE}}} \cdot \frac{\delta_{\mathrm{Xe}}}{\delta_{\mathrm{XE}}}. \tag{29}$$

Similarly, the remaining tangential derivatives are approximated by:

$$\left.\frac{\partial v}{\partial y}\right|_{\mathrm{w}} = \frac{v_{\mathrm{N}} - v_{\mathrm{S}}}{\delta_{\mathrm{YN}} + \delta_{\mathrm{YS}}} \cdot \frac{\delta_{\mathrm{XW}} - \delta_{\mathrm{Xw}}}{\delta_{\mathrm{XW}}} + \frac{v_{\mathrm{NW}} - v_{\mathrm{SW}}}{\delta_{\mathrm{YWNW}} + \delta_{\mathrm{YWSW}}} \cdot \frac{\delta_{\mathrm{Xw}}}{\delta_{\mathrm{XW}}}, \tag{30}$$

$$\left.\frac{\partial w}{\partial z}\right|_{\mathrm{e}} = \frac{w_{\mathrm{F}} - w_{\mathrm{R}}}{\delta_{\mathrm{ZF}} + \delta_{\mathrm{ZR}}} \cdot \frac{\delta_{\mathrm{XE}} - \delta_{\mathrm{Xe}}}{\delta_{\mathrm{XE}}} + \frac{w_{\mathrm{FE}} - w_{\mathrm{RE}}}{\delta_{\mathrm{ZEFE}} + \delta_{\mathrm{ZERE}}} \cdot \frac{\delta_{\mathrm{Xe}}}{\delta_{\mathrm{XE}}}, \tag{31}$$

$$\left.\frac{\partial w}{\partial z}\right|_{\mathrm{w}} = \frac{w_{\mathrm{F}} - w_{\mathrm{R}}}{\delta_{\mathrm{ZF}} + \delta_{\mathrm{ZR}}} \cdot \frac{\delta_{\mathrm{XW}} - \delta_{\mathrm{Xw}}}{\delta_{\mathrm{XW}}} + \frac{w_{\mathrm{FW}} - w_{\mathrm{RW}}}{\delta_{\mathrm{ZWFW}} + \delta_{\mathrm{ZWRW}}} \cdot \frac{\delta_{\mathrm{Xw}}}{\delta_{\mathrm{XW}}}, \tag{32}$$

$$\left.\frac{\partial v}{\partial x}\right|_{\mathrm{n}} = \frac{v_{\mathrm{E}} - v_{\mathrm{W}}}{\delta_{\mathrm{XE}} + \delta_{\mathrm{XW}}} \cdot \frac{\delta_{\mathrm{YN}} - \delta_{\mathrm{Yn}}}{\delta_{\mathrm{YN}}} + \frac{v_{\mathrm{NE}} - v_{\mathrm{NW}}}{\delta_{\mathrm{XNEN}} + \delta_{\mathrm{XNWN}}} \cdot \frac{\delta_{\mathrm{Yn}}}{\delta_{\mathrm{YN}}}, \tag{33}$$

$$\left.\frac{\partial v}{\partial x}\right|_{\mathrm{s}} = \frac{v_{\mathrm{E}} - v_{\mathrm{W}}}{\delta_{\mathrm{XE}} + \delta_{\mathrm{XW}}} \cdot \frac{\delta_{\mathrm{YS}} - \delta_{\mathrm{Ys}}}{\delta_{\mathrm{YS}}} + \frac{v_{\mathrm{SE}} - v_{\mathrm{SW}}}{\delta_{\mathrm{XSES}} + \delta_{\mathrm{XSWS}}} \cdot \frac{\delta_{\mathrm{Ys}}}{\delta_{\mathrm{YS}}}, \tag{34}$$

$$\left.\frac{\partial w}{\partial x}\right|_{\mathrm{f}} = \frac{w_{\mathrm{E}} - w_{\mathrm{W}}}{\delta_{\mathrm{XE}} + \delta_{\mathrm{XW}}} \cdot \frac{\delta_{\mathrm{ZF}} - \delta_{\mathrm{Zf}}}{\delta_{\mathrm{ZF}}} + \frac{w_{\mathrm{FE}} - w_{\mathrm{FW}}}{\delta_{\mathrm{XFEF}} + \delta_{\mathrm{XFWF}}} \cdot \frac{\delta_{\mathrm{Zf}}}{\delta_{\mathrm{ZF}}}, \tag{35}$$

$$\left.\frac{\partial w}{\partial x}\right|_{\mathrm{r}} = \frac{w_{\mathrm{E}} - w_{\mathrm{W}}}{\delta_{\mathrm{XE}} + \delta_{\mathrm{XW}}} \cdot \frac{\delta_{\mathrm{ZR}} - \delta_{\mathrm{Zr}}}{\delta_{\mathrm{ZR}}} + \frac{w_{\mathrm{RE}} - w_{\mathrm{RW}}}{\delta_{\mathrm{XRER}} + \delta_{\mathrm{XRWR}}} \cdot \frac{\delta_{\mathrm{Zr}}}{\delta_{\mathrm{ZR}}}. \tag{36}$$

The distances in these equations are shown in Figs. 3–6. Substituting (20)–(25) and (29)–(36) into (19) yields

$$\begin{aligned}\frac{\mathrm{d}^2 u_{\mathrm{P}}}{\mathrm{d}t^2} &= -P_1 u_{\mathrm{P}} + \mathcal{E}_1 u_{\mathrm{E}} + W_1 u_{\mathrm{W}} + N_1 u_{\mathrm{N}} + S_1 u_{\mathrm{S}} \\ &\quad + F_1 u_{\mathrm{F}} + R_1 u_{\mathrm{R}} + B_{11}(v_{\mathrm{N}} - v_{\mathrm{S}}) + B_{12}(v_{\mathrm{NE}} - v_{\mathrm{SE}}) \\ &\quad - B_{13}(v_{\mathrm{NW}} - v_{\mathrm{SW}}) + B_{14}(v_{\mathrm{E}} - v_{\mathrm{W}}) + B_{15}(v_{\mathrm{NE}} - v_{\mathrm{NW}}) \\ &\quad - B_{16}(v_{\mathrm{SE}} - v_{\mathrm{SW}}) + B_{17}(w_{\mathrm{F}} - w_{\mathrm{R}}) + B_{18}(w_{\mathrm{FE}} - w_{\mathrm{RE}}) \\ &\quad - B_{19}(w_{\mathrm{FW}} - w_{\mathrm{RW}}) + B_{110}(w_{\mathrm{E}} - w_{\mathrm{W}}) \\ &\quad + B_{111}(w_{\mathrm{FE}} - w_{\mathrm{FW}}) + B_{112}(w_{\mathrm{RE}} - w_{\mathrm{RW}}).\end{aligned} \tag{37}$$

Refer to Appendix B for the coefficients in (37). Eq. (37) is an ODE for u, the displacement in the x direction, of an interior control volume. The second and third components of (13) are approximated in a similar way, resulting in ODEs for v and w, the displacements in the y and z directions, respectively:

$$\begin{aligned}\frac{\mathrm{d}^2 v_{\mathrm{P}}}{\mathrm{d}t^2} &= -P_2 v_{\mathrm{P}} + \mathcal{E}_2 v_{\mathrm{E}} + W_2 v_{\mathrm{W}} + N_2 v_{\mathrm{N}} + S_2 v_{\mathrm{S}} \\ &\quad + F_2 v_{\mathrm{F}} + R_2 v_{\mathrm{R}} + B_{21}(u_{\mathrm{N}} - u_{\mathrm{S}}) + B_{22}(u_{\mathrm{NE}} - u_{\mathrm{SE}}) \\ &\quad - B_{23}(u_{\mathrm{NW}} - u_{\mathrm{SW}}) + B_{24}(u_{\mathrm{E}} - u_{\mathrm{W}}) + B_{25}(u_{\mathrm{NE}} - u_{\mathrm{NW}}) \\ &\quad - B_{26}(u_{\mathrm{SE}} - u_{\mathrm{SW}}) + B_{27}(w_{\mathrm{F}} - w_{\mathrm{R}}) + B_{28}(w_{\mathrm{FN}} - w_{\mathrm{RN}}) \\ &\quad - B_{29}(w_{\mathrm{FS}} - w_{\mathrm{RS}}) + B_{210}(w_{\mathrm{N}} - w_{\mathrm{S}}) \\ &\quad + B_{211}(w_{\mathrm{FN}} - w_{\mathrm{FS}}) + B_{212}(w_{\mathrm{RN}} - w_{\mathrm{RS}}),\end{aligned} \tag{38}$$

$$\begin{aligned}\frac{\mathrm{d}^2 w_{\mathrm{P}}}{\mathrm{d}t^2} &= -P_3 w_{\mathrm{P}} + \mathcal{E}_3 w_{\mathrm{E}} + W_3 w_{\mathrm{W}} + N_3 w_{\mathrm{N}} + S_3 w_{\mathrm{S}} \\ &\quad + F_3 w_{\mathrm{F}} + R_3 w_{\mathrm{R}} + B_{31}(u_{\mathrm{F}} - u_{\mathrm{R}}) + B_{32}(u_{\mathrm{FE}} - u_{\mathrm{RE}}) \\ &\quad - B_{33}(u_{\mathrm{FW}} - u_{\mathrm{RW}}) + B_{34}(u_{\mathrm{E}} - u_{\mathrm{W}}) + B_{35}(u_{\mathrm{FE}} - u_{\mathrm{FW}}) \\ &\quad - B_{36}(u_{\mathrm{RE}} - u_{\mathrm{RW}}) + B_{37}(v_{\mathrm{F}} - v_{\mathrm{R}}) + B_{38}(v_{\mathrm{FN}} - v_{\mathrm{RN}}) \\ &\quad - B_{39}(v_{\mathrm{FS}} - v_{\mathrm{RS}}) + B_{310}(v_{\mathrm{N}} - v_{\mathrm{S}}) \\ &\quad + B_{311}(v_{\mathrm{FN}} - v_{\mathrm{FS}}) + B_{312}(v_{\mathrm{RN}} - v_{\mathrm{RS}}).\end{aligned} \tag{39}$$

Refer to Appendix B for the coefficients in (38) and (39).

2) Boundary Control Volumes: Returning to (19), one needs to approximate the normal and tangential derivatives averaged over a face. For an interior control volume, this was done using the average displacements at neighboring volumes. A boundary control volume has at least one face which is on the boundary of the piezoelectric material. Because one cannot refer to the displacements averaged over the neighboring control volume on the other side of this face, instead one refers to the displacements averaged over the face itself.

The three displacements averaged over a boundary face are determined by the three boundary conditions on the face. For example, consider an East face on the boundary with the boundary conditions specifying the normal and tangential stresses

$$T_1 = t_1, \tag{40}$$

$$T_6 = t_6, \tag{41}$$

$$T_5 = t_5. \tag{42}$$

Using the values t_1, t_5, and t_6, one can approximate u_{E}, the displacement in the x direction averaged over the East face, and v_{E} and w_{E}, the displacements in the y and z directions averaged over the East face, respectively. These average displacements are then used directly in the ODEs (37)–(39). Boundary conditions corresponding to a free face would be $t_1 = t_5 = t_6 = 0$. Boundary conditions corresponding to a face restrained from moving in the normal direction would be zero displacement in the normal direction and zero stress in the tangential directions. At an East face, this would correspond to $u_{\mathrm{E}} = 0$, $t_5 = 0$, and

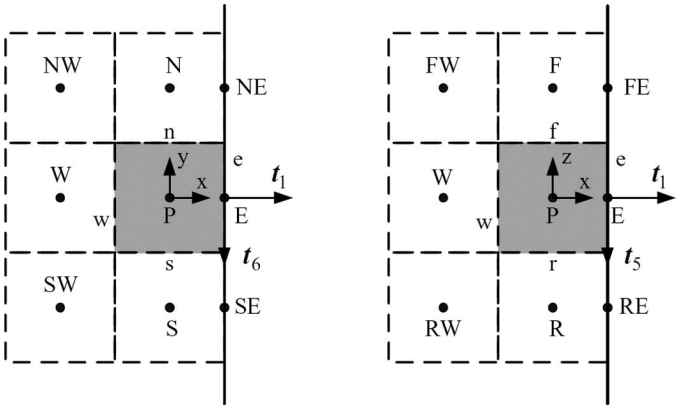

Fig. 8. Control volume placed at the East boundary.

$t_6 = 0$. If the East face is constrained from moving, this would correspond to $u_{\mathrm{E}} = v_{\mathrm{E}} = w_{\mathrm{E}} = 0$.

One might hope that the three boundary conditions on a boundary face would yield three equations which could then be solved for the three displacements. In fact, the three equations involve (unknown) displacements averaged over neighboring boundary faces. As a result, all the boundary faces have to be considered at once, resulting in a system of $6(n_x n_y + n_y n_z + n_z n_x)$ linear equations that reflect the boundary conditions on the $2(n_x n_y + n_y n_z + n_z n_x)$ boundary faces. Solving this system determines the average displacements on all the boundary faces, which are then used in the ODEs (37)–(39).

In the following, the three types of boundary control volumes are considered: face volumes (have one face on the boundary of the piezoelectric material), edge volumes (two faces in common), and corner volumes (three faces in common).

3) Face Volume With Face on the East Boundary: Fig. 8 shows an example of a control volume which has its face on the East side of the boundary of the piezoelectric material. By Figs. 2 and 7, such a control volume will have the tensor components T_1, T_5, and T_6 given by boundary conditions, denoted t_1, t_5, and t_6. These components are expressed in terms of the strains and the electric field within the control volume (17). The resulting equations are

$$c_{11}S_{1\mathrm{e}} + c_{12}S_{2\mathrm{e}} + c_{13}S_{3\mathrm{e}} - e_{31}E_3 = t_1, \tag{43}$$

$$c_{66}S_{6\mathrm{e}} = t_6, \tag{44}$$

$$c_{55}S_{5\mathrm{e}} = t_5. \tag{45}$$

As before, the strain terms in (43)–(45) are expressed in terms of the normal and tangential derivatives of the displacements averaged over the face, as shown in [20]:

$$c_{11}\left.\frac{\partial u}{\partial x}\right|_{\mathrm{e}} + c_{21}\left.\frac{\partial v}{\partial y}\right|_{\mathrm{e}} + c_{31}\left.\frac{\partial w}{\partial z}\right|_{\mathrm{e}} - e_{31}E_3 = t_1, \tag{46}$$

$$c_{66}\left(\left.\frac{\partial u}{\partial y}\right|_{\mathrm{e}} + \left.\frac{\partial v}{\partial x}\right|_{\mathrm{e}}\right) = t_6, \tag{47}$$

$$c_{55}\left(\left.\frac{\partial u}{\partial z}\right|_{\mathrm{e}} + \left.\frac{\partial w}{\partial x}\right|_{\mathrm{e}}\right) = t_5. \tag{48}$$

In (46)–(48), the normal and tangential derivatives averaged over the face are approximated by linear functions of the displacements in the control volumes adjacent to these boundaries with expressions similar to equations (20)–(25) and (29)–(36). This results in

$$u_{\mathrm{E}} = u_{\mathrm{P}} - A_{\mathrm{E1}}(v_{\mathrm{NE}} - v_{\mathrm{SE}}) - A_{\mathrm{E2}}(w_{\mathrm{FE}} - w_{\mathrm{RE}}) + A_{\mathrm{E3}}E_3\frac{\delta_{\mathrm{XE}}}{c_{11}}t_1, \tag{49}$$

$$v_{\mathrm{E}} = v_{\mathrm{P}} - A_{\mathrm{E4}}(u_{\mathrm{NE}} - u_{\mathrm{SE}}) + \frac{\delta_{\mathrm{XE}}}{c_{66}}t_6, \tag{50}$$

$$w_{\mathrm{E}} = w_{\mathrm{P}} - A_{\mathrm{E5}}(u_{\mathrm{FE}} - u_{\mathrm{RE}}) + \frac{\delta_{\mathrm{XE}}}{c_{55}}t_5. \tag{51}$$

The coefficients in (49)–(51) are given in Appendix B. In using equation (20), the displacement u_{E} corresponds to the displacement in the x direction averaged over the East face (see Fig. 8) and δ_{XE} is the distance from the midpoint of the control volume to the East face (denoted δ_{Xe}). Similarly, in using equation (31), because δ_{XE} equals δ_{Xe}, one is really using the approximation

$$\left.\frac{\partial w}{\partial z}\right|_{\mathrm{e}} = \frac{w_{\mathrm{FE}} - w_{\mathrm{RE}}}{\delta_{\mathrm{ZEFE}} + \delta_{\mathrm{ZERE}}}. \tag{52}$$

Note that the electric field E_3 appears in the (49) for u_{E}. Because the electric field is assumed uniform in space, leading to cancellations as in (18), it enters only via the boundary conditions.

Appendix C addresses the remaining face volumes (West, North, South, Front, and Rear) as well as the edge volumes and corner volumes.

C. Step 3: Solution of Equations

The piezoelectric plate is divided into $n_x n_y n_z$ control volumes resulting in $3n_x n_y n_z$ second-order ODEs (37)–(39) for the average displacements of the control volumes. These displacements are written as a vector $\mathbf{X}$ of length $3n_x n_y n_z$:

$$\mathbf{X} = \begin{bmatrix} u_{\mathrm{P}} \\ v_{\mathrm{P}} \\ w_{\mathrm{P}} \end{bmatrix}_{\text{in all control volumes}}. \tag{53}$$

To reduce the system of second-order equations to a system of first-order equations, introduce $\mathbf{Y}$:

$$\mathbf{Y} = \begin{bmatrix} \frac{\mathrm{d}u_{\mathrm{P}}}{\mathrm{d}t} \\ \frac{\mathrm{d}v_{\mathrm{P}}}{\mathrm{d}t} \\ \frac{\mathrm{d}w_{\mathrm{P}}}{\mathrm{d}t} \end{bmatrix}_{\text{in all control volumes}}. \tag{54}$$

The second-order differential equations (37)–(39) depend not only on the displacements in the control volumes, but also on the displacements at the boundaries. The vector $\mathbf{U}$, of length $6(n_x n_y + n_y n_z + n_z n_x)$, containing the average displacements at the boundary faces, is defined as:

$$\mathbf{U} = \begin{bmatrix} u \\ v \\ w \end{bmatrix}_{\text{boundaries}}. \tag{55}$$

The second-order system is then written in the vector-matrix form:

$$\dot{\mathbf{X}} = \mathbf{Y} \tag{56}$$

$$\dot{\mathbf{Y}} = \mathbf{A}\mathbf{X} + \mathbf{B}\mathbf{U}, \tag{57}$$

where $\mathbf{A}$ and $\mathbf{B}$ contain the coefficients of the displacements in the differential equations (37)–(39). The dot on $\mathbf{X}$ and $\mathbf{Y}$ represents differentiation with respect to time. The values of the displacements at the boundaries are written as a linear combination of the displacements in the boundary control volumes, the displacements at the boundaries, the stresses at the boundaries, and the forcing terms produced by the electric field, as shown in (49)–(51) and (162)–(176):

$$\mathbf{U} = \mathbf{C}\mathbf{X} + \mathbf{D}\mathbf{U} + \mathbf{F} + \mathcal{T}. \tag{58}$$

In (58), $\mathbf{F}$ is the forcing vector that contains the forcing terms produced by the electric field. $\mathcal{T}$ is the vector that contains the prescribed stresses from the boundary conditions such as t_1 and the like. $\mathbf{C}$ and $\mathbf{D}$ contain the coefficients of the displacements in the boundary equations. Eqs. (56)–(58) can be represented in an equivalent circuit form in a direct and intuitive manner [8]. This would be helpful for use in a controller. See [21], [22], and [23] for circuit formulations of FEM models.

Solving (58) for $\mathbf{U}$ and substituting into (57), the first-order system (56), (57) becomes:

$$\begin{bmatrix} \dot{\mathbf{X}} \\ \dot{\mathbf{Y}} \end{bmatrix} = \begin{bmatrix} 0 & \mathbf{I} \\ \mathbf{A} + \mathbf{B}(\mathbf{I} - \mathbf{D})^{-1}\mathbf{C} & 0 \end{bmatrix} \begin{bmatrix} \mathbf{X} \\ \mathbf{Y} \end{bmatrix} + \begin{bmatrix} 0 \\ \mathbf{B}(\mathbf{I} - \mathbf{D})^{-1}(\mathbf{F} + \mathcal{T}) \end{bmatrix}. \tag{59}$$

Given initial data, (59) is then solved in Matlab (The MathWorks, Natick, MA).

To find the eigenmodes and eigenfrequencies of the piezoelectric plate, one computes the eigenvalues and eigenvectors of the system matrix A_1

$$\mathbf{A}_1 = \begin{bmatrix} 0 & \mathbf{I} \\ \mathbf{A} + \mathbf{B}(\mathbf{I} - \mathbf{D})^{-1}\mathbf{C} & 0 \end{bmatrix}. \tag{60}$$

One advantage of the FVM model in comparison with a finite element implementation via COMSOL, for example, is that the FVM approach allows one to do such a study of the system matrix $\mathbf{A}_1$.

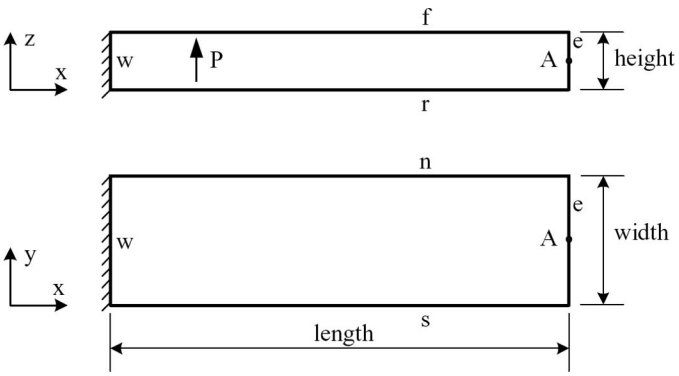

Fig. 9. Piezoelectric plate with West face held fixed, other faces free.

V. Simulations

Simulations are presented for a piezoelectric plate shown in Fig. 9. The plate is made from PIC151 material from Physik Instrumente (Karlsruhe, Germany); its material properties are given in Appendix A. The dimensions of the piezoelectric plate are length = 0.070 m, width = 0.025 m, and height 0.0005 m. The simulations were performed on a Toshiba Satellite P300–0K5 (Tokyo, Japan) with an Intel Core Duo Processor P7350 (2.0 GHz, 1066 MHz FSB, 3 MB L2 Cache; Santa Clara, CA) and 4 GB of RAM running Windows 7 (Microsoft Corp., Redmond, WA).

A. Static Analysis

The West face of the plate is restrained from moving in the x direction but it can freely move in the y and z directions: the boundary conditions are $u = 0$, and the tangential stresses (T_5, T_6) equal zero. On all the other faces of the plate the boundary conditions are zero normal and tangential stresses. The coordinates are chosen so that the midpoint of the West face of the plate is $(0, 0, 0)$. A 100 V dc voltage is applied to the piezoelectric plate. The corresponding electric field is $E_3 = -100/.0005$ V/m. The exact static solution is

$$\begin{pmatrix} u(x,y,z) \\ v(x,y,z) \\ w(x,y,z) \end{pmatrix} = \begin{pmatrix} 4.2908 \times 10^{-5} x \\ 4.2908 \times 10^{-5} y \\ -8.4654 \times 10^{-5} z \end{pmatrix}. \tag{61}$$

The static solution corresponds to a plate that expands uniformly in the x and y directions and compresses uniformly in the z direction in response to the electric field; after the electric field is turned on, the brick-shaped piezoelectric material deforms to a somewhat shorter, somewhat longer and wider brick-shape.

This exact solution is used to test the FVM approximation. A uniform grid is chosen and the static solution is computed via

$$(\mathbf{A} + \mathbf{B}(\mathbf{I} - \mathbf{D})^{-1}\mathbf{C})X = -\mathbf{B}(\mathbf{I} - \mathbf{D})^{-1}(\mathbf{F} + \mathcal{T}), \tag{62}$$

TABLE I. THE DISPLACEMENT IN THE x DIRECTION, u, AT POINT A, AS CALCULATED WITH THE FVM MODEL, COMPARED WITH THE EXACT SOLUTION.

$n_x n_y n_z$	Displacement u at A (μm)	Relative error (%)
$1 = 1 \cdot 1 \cdot 1$	3.0035	4.8×10^{-11}
$27 = 3 \cdot 3 \cdot 3$	3.0035	3.7×10^{-10}

[see (59)]. The value of the resulting displacement in the x direction, u, at the midpoint of the East face (location A) is compared with the values from the exact solution (61). That is, the displacement u in (61) is evaluated at $x = 0.7$, yielding $u = 3.0035$ μm. Table I presents these values and the relative errors; the FVM approximation of the solution is correct up to round-off error. Indeed, because the exact solution is linear and the approximations of the derivatives are second-order accurate, it is expected that the code should capture this exact solution perfectly.

How the FVM model compares with a finite element method (FEM) is studied via COMSOL's FEM implementation. COMSOL computes (3) and (4) with the boundary conditions for the displacement as given above and with the following boundary conditions for the electric field: zero flux density on the E/W/N/S faces and constant on the F and R faces. This results in an electric field that is zero in the x and y directions and constant in the z direction. (The boundary conditions are chosen to eliminate fringing electrical flux.) Because the piezoelectric plate shown in Fig. 9 has a simple geometry, the COMSOL mode[3] Piezo Solid 3-D is used with linear brick elements and no electrical or mechanical losses. Losses are neglected in the COMSOL implementation to allow a fair comparison to the FVM model, which was developed without losses.

To compare the FVM model to COMSOL's FEM implementation, one needs to choose boundary conditions that do not result in an exact solution which has displacements that are linear in x, y, and z. For example, the West face is restrained from moving in any direction: $u = v = w = 0$ and on all the other faces the boundary conditions are zero normal and tangential stresses. As above, a 100 V dc voltage is applied to the piezoelectric plate. The static solution is computed for the FVM model and the displacement in the x direction, u, is found at the point A (see Fig. 9). This is compared with the limiting value of 3.0472 μm. The limiting value is taken from a well-resolved COMSOL run with 234 252 degrees of freedom.

For the FVM simulations, the piezoelectric material is divided into control cells of uniform width, length, and height. The values of n_x, n_y, and n_z are chosen as follows. For each triple (n_x, n_y, n_z) the length, width, and height of the control volume are $(.07/n_x, .025/n_y, .0005/n_z)$. The n_x and n_y are chosen so that the length and width are similar to one another. The piezoelectric material is so thin that even with $n_z = 1$, the height of the control cell is smaller than its length and width. For this reason, n_z is held at the value 1 and n_x and n_y are increased until the control cell's length and width are comparable to the height, at which point n_z would be increased.

It is not obvious how to apply the boundary conditions to a material that has edges and corners. The West face is bounded by four edges, each shared with another face. The FVM discretization needs values for the displacements on the edges; these are determined by the boundary conditions chosen for the edges. In the following, two choices are considered. The first choice (Type 1) assigns the four bounding edges the same boundary conditions as for the West face: $u = v = w = 0$. That is, the edges are glued down with infinite strength, just like the West face, and cannot move in any direction. The second choice (Type 2) assigns the four bounding edges zero displacement in the x direction ($u = 0$)—the edges cannot move toward or away from the wall that the West face is glued to. However, the displacements in the y and z directions, v and w, are not all constrained to zero displacement. For the edges shared by the West and Rear faces or by the West and Front faces, w_{RW} and w_{FW} are determined by extrapolation, see equations (182) and (180) respectively. The algorithm does not need values for v on these edges and so no assumptions are made on these. For the edges shared by the West and South faces or by the West and North faces, v_{SW} and v_{NW} are determined by extrapolation, see equations (198) and (194), respectively. No values for w are needed on these edges.

Table II presents the displacements in the x direction, u, at the point A (see Fig. 9) and the relative errors as computed using the FVM model using both the Type 1 and Type 2 boundary conditions. Similarly, the static solution is computed via COMSOL and the displacements and relative errors are presented in Table III. The COMSOL simulations were performed using the linear solver Direct (SPOOLES) with the relative tolerance set to 1.0E−6 and the maximum number of iterations set to 25; all other settings are left at their defaults. Like the FVM model, parallelepipeds are used as the elements.

Fig. 10 presents the displacement in the x direction, u, at the point A for a larger number of runs of the FVM model with Type 1 and Type 2 boundary conditions as well as COMSOL's FEM model. The horizontal axis is the number of degrees of freedom: $3n_x n_y n_z$ for the FVM models and as given by COMSOL for the FEM model. The horizontal dashed lines in the figure denote the limiting value 3.0472 μm and a 2% error window about this value. From the graph, COMSOL's FEM model yields displacements within 2% of the limiting value using about 940 degrees of freedom. The FVM model with Type 1 boundary conditions yields displacements within 2% using about 430 degrees of freedom. The FVM model with Type 2 boundary conditions yields displacements that are within 2% of the limiting value for all values of n_x, n_y, and n_z tested, starting with $n_x = n_y = n_z = 1$.

Tables II and III also show the simulation times for the FVM and COMSOL simulations. The FVM simulation

[3]The exact path is Application Modes/MEMS Module/Structural Mechanics/Piezo Solid/

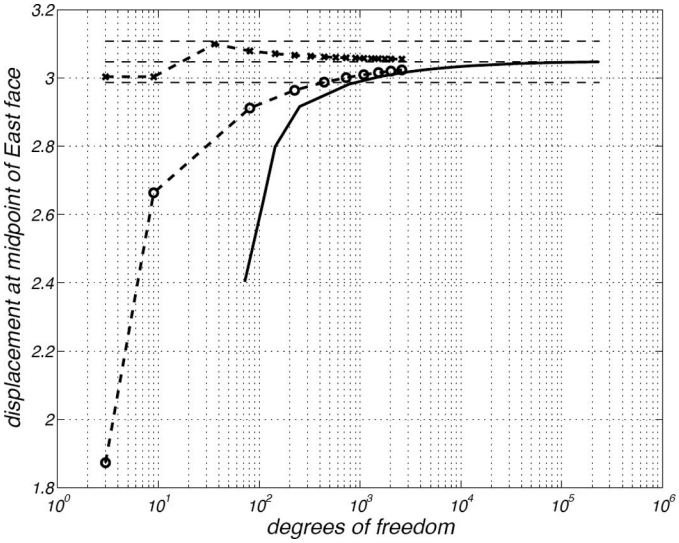

Fig. 10. The horizontal axis denotes the number of degrees of freedom for the FVM and the COMSOL models. The vertical axis denotes u, the displacement in the x direction, at the point A. Solid line: data from COMSOL, dashed line with circles: FVM model with Type 1 boundary conditions, dashed line with ×s: FVM model with Type 2 boundary conditions, horizontal dashed lines: 3.0472 μm and 3.0472 μm ±2%.

times are significantly longer than the COMSOL ones. By timing the separate subroutines of our code, we found that more than 90% of the run time is spent constructing the matrices A, B, C, and D (59). The code was not written with speed as a goal; indeed, these large matrices were constructed using nested ***for*** loops (which increases the simulation times dramatically) and were not handled using Matlab's sparse matrix data structure. To reduce the simulation times, one could code these matrices directly into a sparse matrix data structure and also use Matlab's MEX files to speed up these parts of the code.

B. Eigenfrequency Analysis

For the eigenfrequency analysis, the West face is restrained from moving in any direction and the other faces have zero normal and tangential stresses. For the FVM model, one computes the eigenvectors and eigenvalues of the system matrix $\mathbf{A}_1$, see (60). For each eigenvector, one reconstructs a solution of the form $e^{i\omega t}(u, v, w)$. One first culls out those eigenvectors that result in solutions that have any displacement in the y or z directions; the remaining eigenvectors result in solutions with $v = w = 0$. From these, one then selects the eigenvector for which u has a single maximum (or minimum) value. The eigenvalue (or frequency) corresponding to this eigenvector (or mode), as computed with different numbers of degrees of freedom, is shown in Table IV. In the following, this frequency is called the fundamental frequency.

The analogous fundamental frequency, as calculated with COMSOL, is shown in Table V. The computations are compared with the limiting value of 9951 Hz, taken from a well-resolved COMSOL run with 8360 degrees of freedom. The results shown in Tables IV and V are also plotted in Fig. 11. For the eigenfrequency analysis, the number of degrees of freedom for the FVM model is $6n_x$-n_yn_z.

Fig. 11 presents the fundamental frequency for the FVM model with Type 1 and Type 2 boundary conditions as well as COMSOL's FEM model. The horizontal axis is the number of degrees of freedom. Horizontal dashed lines in the figure mark the limiting value of 9951 Hz and a 2% error window about this value. From the graph, both COMSOL's FEM model and the FVM model with Type 1 boundary conditions yield frequencies within 2% of the limiting value using about 280 degrees of freedom. The FVM model with Type 2 boundary conditions yields

TABLE II. THE DISPLACEMENT IN THE x DIRECTION, u, AT POINT A, AS CALCULATED WITH THE FVM MODEL FOR DIFFERENT NUMBERS OF DEGREES OF FREEDOM (DOF), COMPARED WITH THE LIMITING VALUE (3.0472 μM).

		Type 1 boundary cond.			Type 2 boundary cond.		
Volume	DoF	Displ. (μm)	Rel. error (%)	Sim. time (s)	Displ. (μm)	Rel. error (%)	Sim. time (s)
3	9	2.6634	12.6	1.17	3.0035	1.43	1.17
27	81	2.9118	4.44	3.72	3.0789	1.04	3.70
147	441	2.9874	1.96	36.7	3.0615	0.469	36.7
507	1521	3.0156	1.04	312	3.0562	0.296	312
675	2025	3.0201	0.891	535	3.0555	0.271	530

TABLE III. THE DISPLACEMENT IN THE x DIRECTION, u, AT POINT A, AS CALCULATED WITH COMSOL FOR DIFFERENT NUMBERS OF DEGREES OF FREEDOM (DOF), COMPARED WITH THE LIMITING VALUE (3.0472 μM).

Volume	DoF	Displ. (μm)	Rel. error (%)	Sim. time (s)
4	72	2.4028	21.1	0.06
12	144	2.7986	8.17	0.08
96	780	2.9819	2.15	0.10
384	2700	3.0160	1.03	0.27
864	5772	3.0276	0.645	0.63

TABLE IV. FUNDAMENTAL FREQUENCY, AS CALCULATED WITH THE FVM METHOD FOR DIFFERENT NUMBERS OF DEGREES OF FREEDOM (DOF), COMPARED WITH THE LIMITING VALUE (9951 HZ).

	Type 1 boundary cond.		Type 2 boundary cond.	
DoF	Freq. (Hz)	Rel. error (%)	Freq. (Hz)	Rel. error (%)
18	10916	9.70	9898	0.537
162	10231	2.81	9968	0.173
882	10044	0.933	9938	0.129
3042	9985	0.344	9930	0.211
4050	9977	0.258	9929	0.222

TABLE V. FUNDAMENTAL FREQUENCY, AS CALCULATED WITH COMSOL FOR DIFFERENT NUMBERS OF DEGREES OF FREEDOM (DOF), COMPARED WITH THE LIMITING VALUE (9951 HZ).

DoF	Freq. (Hz)	Rel. error (%)
64	10699	7.51
168	10243	2.93
768	10032	0.817
2728	9974	0.234
5888	9957	0.0568

displacements that are within 2% of the limiting value for all values of n_x, n_y, and n_z tested, starting with $n_x = n_y = n_z = 1$.

VI. POST–PROCESSING AND CONTROL

For control purposes, one needs to know the current sinked or sourced by the power supply. This section presents how this can be easily approximated via the sensor equation (2).

As shown in Fig. 12, the piezoelectric plate has two electrodes: one on the Front (F) face and one on the Rear (R) face. An electric potential difference V is applied across the electrodes and an electric field E is created. The electric dipoles inside the piezoelectric material are deformed by the external electric field in such way that bound charges with opposing polarity will be generated at the positive and negative electrodes. The negative charges are generated at the interface with the positive electrode and the positive charges are generated at the interface with the negative electrode. At the interface between the metal and the piezoelectric materials, one can distinguish between two types of electrical charges: 1) the bound charge on the piezoelectric material generated by the deformation of the piezoelectric material or an externally applied voltage, and 2) a free charge in the metal at the metal/piezo interface with a sign that is opposite to the polarity of the bound charge in the piezo material at the metal/piezo interface. The free charge is supplied by the voltage power supply V.

Consider a small box, partially in the piezoelectric material, partly in the metal, as shown in Fig. 13. Applying Gauss' law to this box, one has

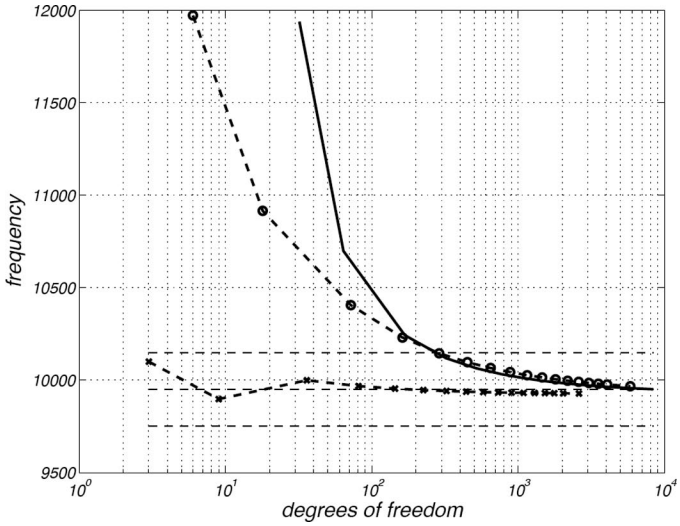

Fig. 11. The horizontal axis denotes the number of degrees of freedom for the FVM and the COMSOL models. The vertical axis denotes the fundamental frequency for the corresponding discretization. Solid line: data from COMSOL, dashed line with circles: FVM model with Type 1 boundary conditions, dashed line with ×s: FVM model with Type 2 boundary conditions, horizontal dashed lines: 9951 Hz and 9951 Hz ±2%.

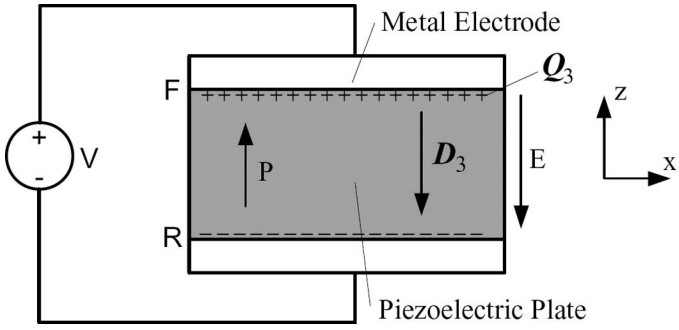

Fig. 12. Electrical boundaries of the piezoelectric plate.

$$\oint_S \mathbf{D}(x, y, z, t) \cdot \mathrm{d}\mathbf{A} = Q(t). \tag{63}$$

In (63), S is the closed surface bounding the box, $\mathbf{D}(x, y, z, t)$ is the electric flux density, $\mathrm{d}\mathbf{A}$ is the differential area of the surface with an outward facing surface normal, and $Q(t)$ is the charge inside the box. The height Δh of the box is taken very small so that the contribution to the integral (63) from the sides of S is negligible. As a result, (63) is approximated by

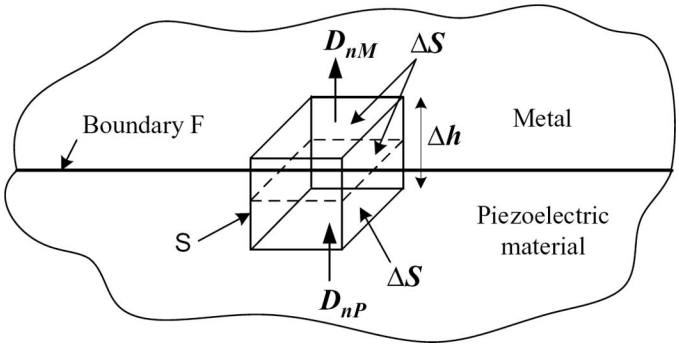

Fig. 13. Metal-piezoelectric plate boundary.

$$\begin{aligned} Q(t) &\approx \int_{\text{top}} \mathbf{D}(\vec{x},t)\cdot\vec{n}_{\text{M}}\mathrm{d}x\mathrm{d}y + \int_{\text{bottom}} \mathbf{D}(\vec{x},t)\cdot\vec{n}_{\text{P}}\mathrm{d}x\mathrm{d}y \\ &= \mathbf{D}|_{\text{top}}(t)\cdot\vec{n}_{\text{M}}\Delta S + \mathbf{D}|_{\text{bottom}}(t)\cdot\vec{n}_{\text{P}}\Delta S. \end{aligned} \tag{64}$$

In (66), $\vec{n}_{\text{M}}$ and $\vec{n}_{\text{P}}$ are the outward facing surface normals at the top and bottom of S, respectively. ΔS is the area of the top (bottom) and the average value of $\mathbf{D}$ on the top is used for $\mathbf{D}|_{\text{top}}(t)$. [$\mathbf{D}|_{\text{bottom}}(t)$ is analogous.]

Because the height Δh of S is very small, the volume charge $Q(t)$ inside S can be approximated by the free charge at the metal-piezoelectric material interface:

$$Q(t) \approx \rho_{\text{S}}(t)\Delta S. \tag{65}$$

In (65), $\rho_{\text{S}}(t)$ is the average free charge density on the metal side of the portion of metal-piezoelectric material interface within the surface S. Combining (65) and (64), dividing by ΔS, and taking ΔS to zero yields:

$$\mathbf{D}|_{\text{M}}(x,y,z,t)\cdot\vec{n}_{\text{M}} + \mathbf{D}|_{\text{P}}(x,y,z,t)\cdot\vec{n}_{\text{P}} = \rho_{\text{S}}(x,y,z,t). \tag{66}$$

In (66), $\mathbf{D}|_{\text{M}}(x,y,z,t)$ is the limit of the electrical flux density as taken from above (going from the metal toward the metal/piezoelectric interface) and $\mathbf{D}|_{\text{P}}(x,y,z,t)$ is the limit of the electrical flux density as taken from below (from within the piezoelectric).

The electric flux density inside the metal is zero and for the Front (F) face of the piezoelectric material $\vec{n}_{\text{P}} = (0,0,-1)$ (see Fig. 13), hence (66) becomes[4]

$$-D_3|_{\text{F}}(x,y,t) \approx \rho_{\text{S}}(x,y,t). \tag{67}$$

Eq. (67) yields the current withdrawn from the power supply:

$$\begin{aligned} i_{\text{F}}(t) &= \frac{\mathrm{d}}{\mathrm{d}t}\int_F \rho_{\text{S}}(x,y,t)\mathrm{d}x\mathrm{d}y \\ &= -\frac{\mathrm{d}}{\mathrm{d}t}\int_F D_3|_{\text{F}}(x,y,t)\mathrm{d}x\mathrm{d}y. \end{aligned} \tag{68}$$

[4]By approximating the normal $\vec{n}_{\text{P}}$ with a constant vector, one is assuming that the piezoelectric material has not significantly deformed. In general, this normal will depend on space and time and one must use (13) (after setting $\mathbf{D}|_M$ to zero).

The sensor equation (17) determines D_3 from the computed solution:

$$D_3|_{\text{F}} = e_{31}\left.\frac{\partial u}{\partial x}\right|_{\text{F}} + e_{32}\left.\frac{\partial v}{\partial y}\right|_{\text{F}} + e_{33}\left.\frac{\partial w}{\partial z}\right|_{\text{F}} + \varepsilon_{33}E_3|_{\text{F}}. \tag{69}$$

In (69), the strains at the boundaries are approximated by linear functions of the average displacements in adjacent control volumes:

$$\begin{aligned} D_3|_{\text{F}} \approx\ & EB_1(u_{\text{FE}} - u_{\text{FW}}) + EB_2(v_{\text{FN}} - v_{\text{FS}}) \\ & + EB_3(w_{\text{F}} - w_{\text{P}}) + \varepsilon_{33}E_3. \end{aligned} \tag{70}$$

The coefficients EB_1 to EB_3 in (70) are given in Appendix B. The total free charge on the Front face of the control volume is found by approximating the integral in (68):

$$Q_{\text{F}}(t) = -\sum_{i=1}^{nx}\sum_{j=1}^{ny}(D_3|_{\text{F}})_{ij}\Delta S_{ij}, \tag{71}$$

where $\Delta S_{ij} = (\delta_{\text{Xe}} + \delta_{\text{Xw}})_i(\delta_{\text{Yn}} + \delta_{\text{Ys}})_j$.

In this way, given the approximate solution (u,v,w) at a sequence of times, one uses (71) to approximate the total free charge on the Front (F) face at those times. One then uses these to approximate the time derivative in (68), resulting in the current flowing across the Front face. There is no current flowing across the four free faces and the current flowing across the Rear face is equal and opposite to that flowing across the Front face.

VII. Conclusions

This paper presents a new modeling technique for piezoelectric devices by using the finite volume method. The modeling technique was developed by starting with the continuum equations (3) and (4) for the piezoelectric material and discretizing them using the finite volume method. This results in a system of second-order ordinary differential equations. Simulations are presented and a comparison of the results with the finite element simulations was performed. The resulting system of ordinary differential equations is easier to consider within a circuit framework; all circuits in electrical engineering are, in effect, an application of the finite volume method. In this paper, a simplifying assumption of constant electric field is made, resulting in a discretization of (3) only. The finite volume method could have been applied to the full system (3) and (4) resulting in a larger system of differential algebraic equations.

Figs. 10 and 11 show that how one chooses to implement the boundary conditions can have a significant impact on how quickly (in terms of degrees of freedom) the simulations converge to the limiting value. Reducing the number of degrees of freedom needed to reach a desired accuracy is quite useful for control purposes. Indeed, for

any control problem it is important to keep the order of the plant model as small as possible because there are real-time implementation issues. The FVM model with the Type 2 boundary conditions does sufficiently well that a further model-order-reduction technique may not be necessary: the observed displacement is within 1% of the limiting value using only 180 degrees of freedom, the fundamental frequency was within 1% of the limiting value using only 18 degrees of freedom. Figs. 10 and 11 suggest that COMSOL's implementation is comparable to the FVM model with Type 1 boundary conditions.

To modify how an FEM model implements boundary conditions at the edges, one would need to make special choices for the elements that occur at edges. One of the strengths of the FVM model presented here is that implementing the boundary conditions is quite straight-forward, allowing one to find a choice which yields a fairly accurate answer with relatively few cells.

Appendix A
Material Properties

The piezoelectric material simulated is PIC151 from Physik Instrumente. The stiffness matrix, $\mathbf{c^E}$, is evaluated at a constant electric field and the dielectric matrix, $\varepsilon^{\mathbf{S}}$, is evaluated at constant strain.

The entries of the dielectric matrix $\varepsilon^{\mathbf{S}}$ in (17) are $\varepsilon_{11} = \varepsilon_{22} = 1110$ and $\varepsilon_{33} = 852$ F/m.

The entries of the stiffness matrix $\mathbf{c^E}$ in (17) are $c_{11} = c_{22} = 1.076 \times 10^{11}$ N/m^2, $c_{33} = 1.004 \times 10^{11}$ N/m^2, $c_{44} = 1.962 \times 10^{10}$ N/m^2, $c_{55} = 1.962 \times 10^{10}$ N/m^2, $c_{66} = 2.224 \times 10^{10}$ N/m^2, $c_{12} = c_{21} = 6.312 \times 10^{10}$ N/m^2, and $c_{13} = c_{31} = c_{23} = c_{32} = 6.385 \times 10^{10}$ N/m^2.

The entries of the electromechanical coupling matrix $\mathbf{e}$ in (17) are $e_{31} = e_{32} = -9.60$ N/(Vm), $e_{33} = 15.10$ N/(Vm), and $e_{15} = e_{24} = 12.00$ N/(Vm).

Appendix B
Equations' Coefficients

$$P_1 = \frac{c_{11}}{\Delta x\rho}\left(\frac{1}{\delta_{\mathrm{XE}}} + \frac{1}{\delta_{\mathrm{XW}}}\right) + \frac{c_{66}}{\Delta y\rho}\left(\frac{1}{\delta_{\mathrm{YN}}} + \frac{1}{\delta_{\mathrm{YS}}}\right) + \frac{c_{55}}{\Delta z\rho}\left(\frac{1}{\delta_{\mathrm{ZF}}} + \frac{1}{\delta_{\mathrm{ZR}}}\right) \tag{72}$$

$$\mathcal{E}_1 = \frac{c_{11}}{\Delta x\rho\delta_{\mathrm{XE}}} \tag{73}$$

$$W_1 = \frac{c_{11}}{\Delta x\rho\delta_{\mathrm{XW}}} \tag{74}$$

$$N_1 = \frac{c_{66}}{\Delta y\rho\delta_{\mathrm{YN}}} \tag{75}$$

$$S_1 = \frac{c_{66}}{\Delta y\rho\delta_{\mathrm{YS}}} \tag{76}$$

$$F_1 = \frac{c_{55}}{\Delta z\rho\delta_{\mathrm{ZF}}} \tag{77}$$

$$R_1 = \frac{c_{55}}{\Delta z\rho\delta_{\mathrm{ZR}}} \tag{78}$$

$$B_{11} = \frac{c_{12}}{\Delta x\rho(\delta_{\mathrm{YN}} + \delta_{\mathrm{YS}})}\left(\frac{\delta_{\mathrm{XE}} - \delta_{\mathrm{Xe}}}{\delta_{\mathrm{XE}}} - \frac{\delta_{\mathrm{XW}} - \delta_{\mathrm{Xw}}}{\delta_{\mathrm{XW}}}\right) \tag{79}$$

$$B_{12} = \frac{c_{12}}{\Delta x\rho(\delta_{\mathrm{YENE}} + \delta_{\mathrm{YESE}})}\frac{\delta_{\mathrm{Xe}}}{\delta_{\mathrm{XE}}} \tag{80}$$

$$B_{13} = \frac{c_{12}}{\Delta x\rho(\delta_{\mathrm{YWNW}} + \delta_{\mathrm{YWSW}})}\frac{\delta_{\mathrm{Xw}}}{\delta_{\mathrm{XW}}} \tag{81}$$

$$B_{14} = \frac{c_{66}}{\Delta y\rho(\delta_{\mathrm{XE}} + \delta_{\mathrm{XW}})}\left(\frac{\delta_{\mathrm{YN}} - \delta_{\mathrm{Yn}}}{\delta_{\mathrm{YN}}} - \frac{\delta_{\mathrm{YS}} - \delta_{\mathrm{Ys}}}{\delta_{\mathrm{YS}}}\right) \tag{82}$$

$$B_{15} = \frac{c_{66}}{\Delta y\rho(\delta_{\mathrm{XNEN}} + \delta_{\mathrm{XNWN}})}\frac{\delta_{\mathrm{Yn}}}{\delta_{\mathrm{YN}}} \tag{83}$$

$$B_{16} = \frac{c_{66}}{\Delta y\rho(\delta_{\mathrm{XSES}} + \delta_{\mathrm{XSWS}})}\frac{\delta_{\mathrm{Ys}}}{\delta_{\mathrm{YS}}} \tag{84}$$

$$B_{17} = \frac{c_{13}}{\Delta x\rho(\delta_{\mathrm{ZF}} + \delta_{\mathrm{ZR}})}\left(\frac{\delta_{\mathrm{XE}} - \delta_{\mathrm{Xe}}}{\delta_{\mathrm{XE}}} - \frac{\delta_{\mathrm{XW}} - \delta_{\mathrm{Xw}}}{\delta_{\mathrm{XW}}}\right) \tag{85}$$

$$B_{18} = \frac{c_{13}}{\Delta x\rho(\delta_{\mathrm{ZEFE}} + \delta_{\mathrm{ZERE}})}\frac{\delta_{\mathrm{Xe}}}{\delta_{\mathrm{XE}}} \tag{86}$$

$$B_{19} = \frac{c_{13}}{\Delta x\rho(\delta_{\mathrm{ZWFW}} + \delta_{\mathrm{ZWRW}})}\frac{\delta_{\mathrm{Xw}}}{\delta_{\mathrm{XW}}} \tag{87}$$

$$B_{110} = \frac{c_{55}}{\Delta z\rho(\delta_{\mathrm{XE}} + \delta_{\mathrm{XW}})}\left(\frac{\delta_{\mathrm{ZF}} - \delta_{\mathrm{Zf}}}{\delta_{\mathrm{ZF}}} - \frac{\delta_{\mathrm{ZR}} - \delta_{\mathrm{Zr}}}{\delta_{\mathrm{ZR}}}\right) \tag{88}$$

$$B_{111} = \frac{c_{55}}{\Delta z\rho(\delta_{\mathrm{XFEF}} + \delta_{\mathrm{XFWF}})}\frac{\delta_{\mathrm{Zf}}}{\delta_{\mathrm{ZF}}} \tag{89}$$

$$B_{112} = \frac{c_{55}}{\Delta z\rho(\delta_{\mathrm{XRER}} + \delta_{\mathrm{XRWR}})}\frac{\delta_{\mathrm{Zr}}}{\delta_{\mathrm{ZR}}} \tag{90}$$

$$P_2 = \frac{c_{66}}{\Delta x\rho}\left(\frac{1}{\delta_{\mathrm{XE}}} + \frac{1}{\delta_{\mathrm{XW}}}\right) + \frac{c_{22}}{\Delta y\rho}\left(\frac{1}{\delta_{\mathrm{YN}}} + \frac{1}{\delta_{\mathrm{YS}}}\right) + \frac{c_{44}}{\Delta z\rho}\left(\frac{1}{\delta_{\mathrm{ZF}}} + \frac{1}{\delta_{\mathrm{ZR}}}\right) \tag{91}$$

$$\mathcal{E}_2 = \frac{c_{66}}{\Delta x\rho\delta_{\mathrm{XE}}} \tag{92}$$

$$W_2 = \frac{c_{66}}{\Delta x\rho\delta_{\mathrm{XW}}} \tag{93}$$

$$N_2 = \frac{c_{22}}{\Delta y\rho\delta_{\mathrm{YN}}} \tag{94}$$

$$S_2 = \frac{c_{22}}{\Delta y\rho\delta_{\mathrm{YS}}} \tag{95}$$

$$F_2 = \frac{c_{44}}{\Delta z\rho\delta_{\mathrm{ZF}}} \tag{96}$$

$$R_2 = \frac{c_{44}}{\Delta z\rho\delta_{\mathrm{ZR}}} \tag{97}$$

$$B_{21} = \frac{c_{66}}{\Delta x\rho(\delta_{\mathrm{YN}} + \delta_{\mathrm{YS}})}\left(\frac{\delta_{\mathrm{XE}} - \delta_{\mathrm{Xe}}}{\delta_{\mathrm{XE}}} - \frac{\delta_{\mathrm{XW}} - \delta_{\mathrm{Xw}}}{\delta_{\mathrm{XW}}}\right) \tag{98}$$

$$B_{22} = \frac{c_{66}}{\Delta x \rho(\delta_{\mathrm{YENE}} + \delta_{\mathrm{YESE}})} \frac{\delta_{\mathrm{Xe}}}{\delta_{\mathrm{XE}}} \tag{99}$$

$$B_{23} = \frac{c_{66}}{\Delta x \rho(\delta_{\mathrm{YWNW}} + \delta_{\mathrm{YWSW}})} \frac{\delta_{\mathrm{Xw}}}{\delta_{\mathrm{XW}}} \tag{100}$$

$$B_{24} = \frac{c_{21}}{\Delta y \rho(\delta_{\mathrm{XE}} + \delta_{\mathrm{XW}})} \left(\frac{\delta_{\mathrm{YN}} - \delta_{\mathrm{Yn}}}{\delta_{\mathrm{YN}}} - \frac{\delta_{\mathrm{YS}} - \delta_{\mathrm{Ys}}}{\delta_{\mathrm{YS}}} \right) \tag{101}$$

$$B_{25} = \frac{c_{21}}{\Delta y \rho(\delta_{\mathrm{XNEN}} + \delta_{\mathrm{XNWN}})} \frac{\delta_{\mathrm{Yn}}}{\delta_{\mathrm{YN}}} \tag{102}$$

$$B_{26} = \frac{c_{21}}{\Delta y \rho(\delta_{\mathrm{XSES}} + \delta_{\mathrm{XSWS}})} \frac{\delta_{\mathrm{Ys}}}{\delta_{\mathrm{YS}}} \tag{103}$$

$$B_{27} = \frac{c_{23}}{\Delta y \rho(\delta_{\mathrm{ZF}} + \delta_{\mathrm{ZR}})} \left(\frac{\delta_{\mathrm{YN}} - \delta_{\mathrm{Yn}}}{\delta_{\mathrm{YN}}} - \frac{\delta_{\mathrm{YS}} - \delta_{\mathrm{Ys}}}{\delta_{\mathrm{YS}}} \right) \tag{104}$$

$$B_{28} = \frac{c_{23}}{\Delta y \rho(\delta_{\mathrm{ZNFN}} + \delta_{\mathrm{ZNRN}})} \frac{\delta_{\mathrm{Yn}}}{\delta_{\mathrm{YN}}} \tag{105}$$

$$B_{29} = \frac{c_{23}}{\Delta y \rho(\delta_{\mathrm{ZSFS}} + \delta_{\mathrm{ZSRS}})} \frac{\delta_{\mathrm{Ys}}}{\delta_{\mathrm{YS}}} \tag{106}$$

$$B_{210} = \frac{c_{44}}{\Delta z \rho(\delta_{\mathrm{YN}} + \delta_{\mathrm{YS}})} \left(\frac{\delta_{\mathrm{ZF}} - \delta_{\mathrm{Zf}}}{\delta_{\mathrm{ZF}}} - \frac{\delta_{\mathrm{ZR}} - \delta_{\mathrm{Zr}}}{\delta_{\mathrm{ZR}}} \right) \tag{107}$$

$$B_{211} = \frac{c_{44}}{\Delta z \rho(\delta_{\mathrm{YFNF}} + \delta_{\mathrm{YFSF}})} \frac{\delta_{\mathrm{Zf}}}{\delta_{\mathrm{ZF}}} \tag{108}$$

$$B_{212} = \frac{c_{44}}{\Delta z \rho(\delta_{\mathrm{YRNR}} + \delta_{\mathrm{YRSR}})} \frac{\delta_{\mathrm{Zr}}}{\delta_{\mathrm{ZR}}} \tag{109}$$

$$P_3 = \frac{c_{55}}{\Delta x \rho} \left(\frac{1}{\delta_{\mathrm{XE}}} + \frac{1}{\delta_{\mathrm{XW}}} \right) + \frac{c_{44}}{\Delta y \rho} \left(\frac{1}{\delta_{\mathrm{YN}}} + \frac{1}{\delta_{\mathrm{YS}}} \right) + \frac{c_{33}}{\Delta z \rho} \left(\frac{1}{\delta_{\mathrm{ZF}}} + \frac{1}{\delta_{\mathrm{ZR}}} \right) \tag{110}$$

$$\mathcal{E}_3 = \frac{c_{55}}{\Delta x \rho \delta_{\mathrm{XE}}} \tag{111}$$

$$W_3 = \frac{c_{55}}{\Delta x \rho \delta_{\mathrm{XW}}} \tag{112}$$

$$N_3 = \frac{c_{44}}{\Delta y \rho \delta_{\mathrm{YN}}} \tag{113}$$

$$S_3 = \frac{c_{44}}{\Delta y \rho \delta_{\mathrm{YS}}} \tag{114}$$

$$F_3 = \frac{c_{33}}{\Delta z \rho \delta_{\mathrm{ZF}}} \tag{115}$$

$$R_3 = \frac{c_{33}}{\Delta z \rho \delta_{\mathrm{ZR}}} \tag{116}$$

$$B_{31} = \frac{c_{55}}{\Delta x \rho(\delta_{\mathrm{ZF}} + \delta_{\mathrm{ZR}})} \left(\frac{\delta_{\mathrm{XE}} - \delta_{\mathrm{Xe}}}{\delta_{\mathrm{XE}}} - \frac{\delta_{\mathrm{XW}} - \delta_{\mathrm{Xw}}}{\delta_{\mathrm{XW}}} \right) \tag{117}$$

$$B_{32} = \frac{c_{55}}{\Delta x \rho(\delta_{\mathrm{ZEFE}} + \delta_{\mathrm{ZERE}})} \frac{\delta_{\mathrm{Xe}}}{\delta_{\mathrm{XE}}} \tag{118}$$

$$B_{33} = \frac{c_{55}}{\Delta x \rho(\delta_{\mathrm{ZWFW}} + \delta_{\mathrm{ZWRW}})} \frac{\delta_{\mathrm{Xw}}}{\delta_{\mathrm{XW}}} \tag{119}$$

$$B_{34} = \frac{c_{31}}{\Delta z \rho(\delta_{\mathrm{XE}} + \delta_{\mathrm{XW}})} \left(\frac{\delta_{\mathrm{ZF}} - \delta_{\mathrm{Zf}}}{\delta_{\mathrm{ZF}}} - \frac{\delta_{\mathrm{ZR}} - \delta_{\mathrm{Zr}}}{\delta_{\mathrm{ZR}}} \right) \tag{120}$$

$$B_{35} = \frac{c_{31}}{\Delta z \rho(\delta_{\mathrm{XFEF}} + \delta_{\mathrm{XFWF}})} \frac{\delta_{\mathrm{Zf}}}{\delta_{\mathrm{ZF}}} \tag{121}$$

$$B_{36} = \frac{c_{31}}{\Delta z \rho(\delta_{\mathrm{XRER}} + \delta_{\mathrm{XRWR}})} \frac{\delta_{\mathrm{Zr}}}{\delta_{\mathrm{ZR}}} \tag{122}$$

$$B_{37} = \frac{c_{44}}{\Delta y \rho(\delta_{\mathrm{ZF}} + \delta_{\mathrm{ZR}})} \left(\frac{\delta_{\mathrm{YN}} - \delta_{\mathrm{Yn}}}{\delta_{\mathrm{YN}}} - \frac{\delta_{\mathrm{YS}} - \delta_{\mathrm{Ys}}}{\delta_{\mathrm{YS}}} \right) \tag{123}$$

$$B_{38} = \frac{c_{44}}{\Delta y \rho(\delta_{\mathrm{ZNFN}} + \delta_{\mathrm{ZNRN}})} \frac{\delta_{\mathrm{Yn}}}{\delta_{\mathrm{YN}}} \tag{124}$$

$$B_{39} = \frac{c_{44}}{\Delta y \rho(\delta_{\mathrm{ZSFS}} + \delta_{\mathrm{ZSRS}})} \frac{\delta_{\mathrm{Ys}}}{\delta_{\mathrm{YS}}} \tag{125}$$

$$B_{310} = \frac{c_{32}}{\Delta z \rho(\delta_{\mathrm{YN}} + \delta_{\mathrm{YS}})} \left(\frac{\delta_{\mathrm{ZF}} - \delta_{\mathrm{Zf}}}{\delta_{\mathrm{ZF}}} - \frac{\delta_{\mathrm{ZR}} - \delta_{\mathrm{Zr}}}{\delta_{\mathrm{ZR}}} \right) \tag{126}$$

$$B_{311} = \frac{c_{32}}{\Delta z \rho(\delta_{\mathrm{YFNF}} + \delta_{\mathrm{YFSF}})} \frac{\delta_{\mathrm{Zf}}}{\delta_{\mathrm{ZF}}} \tag{127}$$

$$B_{312} = \frac{c_{32}}{\Delta z \rho(\delta_{\mathrm{YRNR}} + \delta_{\mathrm{YRSR}})} \frac{\delta_{\mathrm{Zr}}}{\delta_{\mathrm{ZR}}} \tag{128}$$

$$A_{\mathrm{E1}} = \frac{c_{12}}{c_{11}} \frac{\delta_{\mathrm{Xe}}}{\delta_{\mathrm{YENE}} + \delta_{\mathrm{YESE}}} \tag{129}$$

$$A_{\mathrm{E2}} = \frac{c_{13}}{c_{11}} \frac{\delta_{\mathrm{Xe}}}{\delta_{\mathrm{ZEFE}} + \delta_{\mathrm{ZERE}}} \tag{130}$$

$$A_{\mathrm{E3}} = \frac{e_{31} \delta_{\mathrm{XE}}}{c_{11}} \tag{131}$$

$$A_{\mathrm{E4}} = \frac{\delta_{\mathrm{Xe}}}{\delta_{\mathrm{YENE}} + \delta_{\mathrm{YESE}}} \tag{132}$$

$$A_{\mathrm{E5}} = \frac{\delta_{\mathrm{Xe}}}{\delta_{\mathrm{ZEFE}} + \delta_{\mathrm{ZERE}}} \tag{133}$$

$$A_{\mathrm{W1}} = \frac{c_{12}}{c_{11}} \frac{\delta_{\mathrm{Xw}}}{\delta_{\mathrm{YWNW}} + \delta_{\mathrm{YWSW}}} \tag{134}$$

$$A_{\mathrm{W2}} = \frac{c_{13}}{c_{11}} \frac{\delta_{\mathrm{Xw}}}{\delta_{\mathrm{ZWFW}} + \delta_{\mathrm{ZWRW}}} \tag{135}$$

$$A_{\mathrm{W3}} = \frac{e_{31} \delta_{\mathrm{XW}}}{c_{11}} \tag{136}$$

$$A_{\mathrm{W4}} = \frac{\delta_{\mathrm{Xw}}}{\delta_{\mathrm{YWNW}} + \delta_{\mathrm{YWSW}}} \tag{137}$$

$$A_{\mathrm{W5}} = \frac{\delta_{\mathrm{Xw}}}{\delta_{\mathrm{ZWFW}} + \delta_{\mathrm{ZWRW}}} \tag{138}$$

$$A_{\mathrm{N1}} = \frac{\delta_{\mathrm{Yn}}}{\delta_{\mathrm{XNEN}} + \delta_{\mathrm{XNWN}}} \tag{139}$$

$$A_{\mathrm{N2}} = \frac{c_{21}}{c_{22}} \frac{\delta_{\mathrm{Yn}}}{\delta_{\mathrm{XNEN}} + \delta_{\mathrm{XNWN}}} \tag{140}$$

$$A_{N3} = \frac{c_{23}}{c_{22}} \frac{\delta_{Yn}}{\delta_{ZNFN} + \delta_{ZNRN}} \tag{141}$$

$$A_{N4} = \frac{e_{32}\delta_{YN}}{c_{22}} \tag{142}$$

$$A_{N5} = \frac{\delta_{Yn}}{\delta_{ZNFN} + \delta_{ZNRN}} \tag{143}$$

$$A_{S1} = \frac{\delta_{Ys}}{\delta_{XSES} + \delta_{XSWS}} \tag{144}$$

$$A_{S2} = \frac{c_{21}}{c_{22}} \frac{\delta_{Ys}}{\delta_{XSES} + \delta_{XSWS}} \tag{145}$$

$$A_{S3} = \frac{c_{23}}{c_{22}} \frac{\delta_{Ys}}{\delta_{ZSFS} + \delta_{ZSRS}} \tag{146}$$

$$A_{S4} = \frac{e_{32}\delta_{YS}}{c_{22}} \tag{147}$$

$$A_{S5} = \frac{\delta_{Ys}}{\delta_{ZSFS} + \delta_{ZSRS}} \tag{148}$$

$$A_{F1} = \frac{\delta_{Zf}}{\delta_{XFEF} + \delta_{XFWF}} \tag{149}$$

$$A_{F2} = \frac{\delta_{Zf}}{\delta_{YFNF} + \delta_{YFSF}} \tag{150}$$

$$A_{F3} = \frac{c_{31}}{c_{33}} \frac{\delta_{Zf}}{\delta_{XFEF} + \delta_{XFWF}} \tag{151}$$

$$A_{F4} = \frac{c_{32}}{c_{33}} \frac{\delta_{Zf}}{\delta_{YFNF} + \delta_{YFSF}} \tag{152}$$

$$A_{F5} = \frac{e_{33}\delta_{ZF}}{c_{33}} \tag{153}$$

$$A_{R1} = \frac{\delta_{Zr}}{\delta_{XRER} + \delta_{XRWR}} \tag{154}$$

$$A_{R2} = \frac{\delta_{Zr}}{\delta_{YRNR} + \delta_{YRSR}} \tag{155}$$

$$A_{R3} = \frac{c_{31}}{c_{33}} \frac{\delta_{Zr}}{\delta_{XRER} + \delta_{XRWR}} \tag{156}$$

$$A_{R4} = \frac{c_{32}}{c_{33}} \frac{\delta_{Zr}}{\delta_{YRNR} + \delta_{YRSR}} \tag{157}$$

$$A_{R5} = \frac{e_{33}\delta_{ZR}}{c_{33}} \tag{158}$$

$$EB_1 = \frac{e_{31}}{\delta_{XFEF} + \delta_{XFWF}} \tag{159}$$

$$EB_2 = \frac{e_{32}}{\delta_{YFNF} + \delta_{YFSF}} \tag{160}$$

$$EB_3 = \frac{e_{33}}{\delta_{ZF}} \tag{161}$$

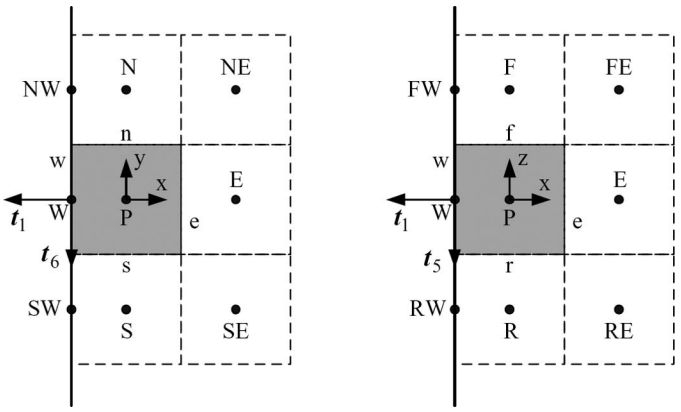

Fig. 14. Control volume placed at the West boundary.

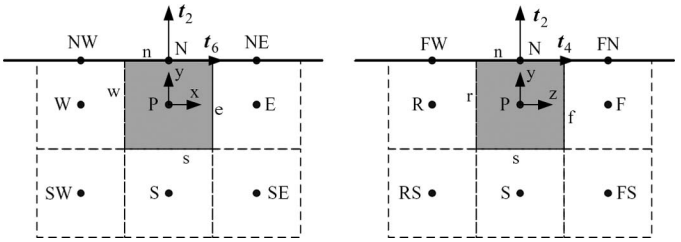

Fig. 15. Control volume placed at the North boundary.

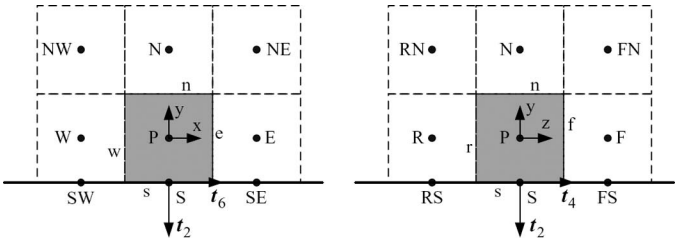

Fig. 16. Control volume placed at the South boundary.

Appendix C
Boundary Equations

A. Face Volumes With Face on the West, North, South, Front, or Rear Boundary

The expressions for the displacements at the West, North, South, Front, and Rear boundaries are obtained in a similar way as the expressions for the displacements at the East boundary. The positions of a control volume at the West, North, South, Front, and Rear boundaries are shown in Figs. 14, 15, 16, 17, and 18. The expressions for the displacements at the West boundary are:

$$u_W = u_P + A_{W1}(v_{NW} - v_{SW}) + A_{W2}(w_{FW} - w_{RW}) - A_{W3}E_3 + \frac{\delta_{XW}}{c_{11}} t_1 \tag{162}$$

$$v_W = v_P + A_{W4}(u_{NW} - u_{SW}) + \frac{\delta_{XW}}{c_{66}} t_6 \tag{163}$$

$$w_W = w_P + A_{W5}(u_{FW} - u_{RW}) + \frac{\delta_{XW}}{c_{55}} t_5 \tag{164}$$

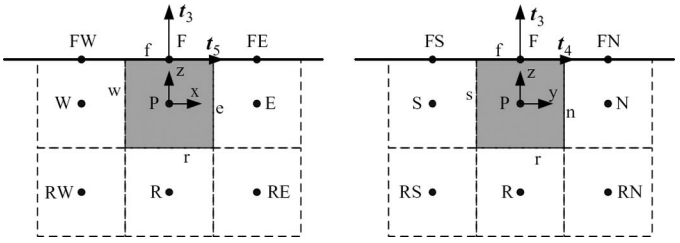

Fig. 17. Control volume placed at the Front boundary.

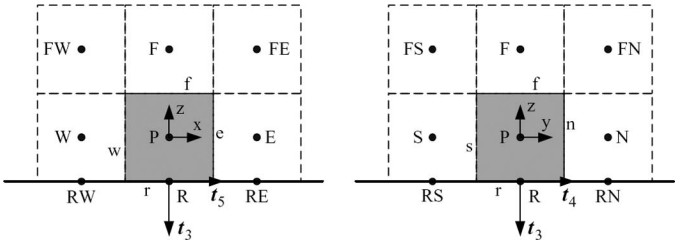

Fig. 18. Control volume placed at the Rear boundary.

The expressions for the displacements at the North boundary are:

$$u_{\mathrm{N}} = u_{\mathrm{P}} - A_{\mathrm{N1}}(v_{\mathrm{NE}} - v_{\mathrm{NW}}) + \frac{\delta_{\mathrm{YN}}}{c_{66}} t_6 \tag{165}$$

$$v_{\mathrm{N}} = v_{\mathrm{P}} - A_{\mathrm{N2}}(u_{\mathrm{NE}} - u_{\mathrm{NW}}) - A_{\mathrm{N3}}(w_{\mathrm{FN}} - w_{\mathrm{RN}}) + A_{\mathrm{N4}} E_3 + \frac{\delta_{\mathrm{YN}}}{c_{22}} t_2 \tag{166}$$

$$w_{\mathrm{N}} = w_{\mathrm{P}} - A_{\mathrm{N5}}(v_{\mathrm{FN}} - v_{\mathrm{RN}}) + \frac{\delta_{\mathrm{YN}}}{c_{44}} t_4 \tag{167}$$

The expressions for the displacements at the South boundary are:

$$u_{\mathrm{S}} = u_{\mathrm{P}} + A_{\mathrm{S1}}(v_{\mathrm{SE}} - v_{\mathrm{SW}}) + \frac{\delta_{\mathrm{YS}}}{c_{66}} t_6 \tag{168}$$

$$v_{\mathrm{S}} = v_{\mathrm{P}} + A_{\mathrm{S2}}(u_{\mathrm{SE}} - u_{\mathrm{SW}}) + A_{\mathrm{S3}}(w_{\mathrm{FS}} - w_{\mathrm{RS}}) - A_{\mathrm{S4}} E_3 + \frac{\delta_{\mathrm{YS}}}{c_{22}} t_2 \tag{169}$$

$$w_{\mathrm{S}} = w_{\mathrm{P}} + A_{\mathrm{S5}}(v_{\mathrm{FS}} - v_{\mathrm{RS}}) + \frac{\delta_{\mathrm{YS}}}{c_{44}} t_4 \tag{170}$$

The expressions for the displacements at the Front boundary are:

$$u_{\mathrm{F}} = u_{\mathrm{P}} - A_{\mathrm{F1}}(w_{\mathrm{FE}} - w_{\mathrm{FW}}) + \frac{\delta_{\mathrm{ZF}}}{c_{55}} t_5 \tag{171}$$

$$v_{\mathrm{F}} = v_{\mathrm{P}} - A_{\mathrm{F2}}(w_{\mathrm{FN}} - w_{\mathrm{FS}}) + \frac{\delta_{\mathrm{ZF}}}{c_{44}} t_4 \tag{172}$$

$$w_{\mathrm{F}} = w_{\mathrm{P}} - A_{\mathrm{F3}}(u_{\mathrm{FE}} - u_{\mathrm{FW}}) - A_{\mathrm{F4}}(v_{\mathrm{FN}} - v_{\mathrm{FS}}) + A_{\mathrm{F5}} E_3 + \frac{\delta_{\mathrm{ZF}}}{c_{33}} t_3 \tag{173}$$

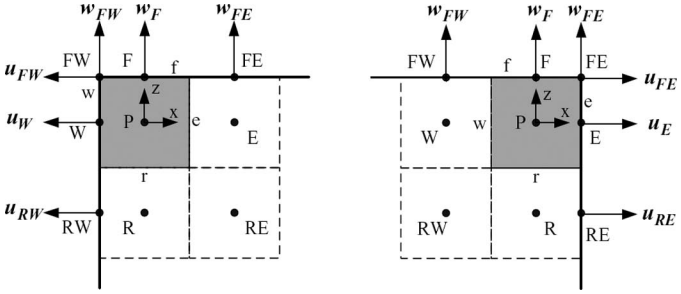

Fig. 19. Control volume placed at the Front-West or Front-East boundaries.

The expressions for the displacements at the Rear boundary are:

$$u_{\mathrm{R}} = u_{\mathrm{P}} + A_{\mathrm{R1}}(w_{\mathrm{RE}} - w_{\mathrm{RW}}) + \frac{\delta_{\mathrm{ZR}}}{c_{55}} t_5 \tag{174}$$

$$v_{\mathrm{R}} = v_{\mathrm{P}} + A_{\mathrm{R2}}(w_{\mathrm{RN}} - w_{\mathrm{RS}}) + \frac{\delta_{\mathrm{ZR}}}{c_{44}} t_4 \tag{175}$$

$$w_{\mathrm{R}} = w_{\mathrm{P}} + A_{\mathrm{R3}}(u_{\mathrm{RE}} - u_{\mathrm{RW}}) + A_{\mathrm{R4}}(v_{\mathrm{RN}} - v_{\mathrm{RS}}) - A_{\mathrm{R5}} E_3 + \frac{\delta_{\mathrm{ZR}}}{c_{33}} t_3 \tag{176}$$

The coefficients in (162)–(176) are given in Appendix B.

B. Edge Volume With Faces on the Front and West Boundaries or the Front and East Boundaries

Refer to Fig. 19 for the location of the control volume in these two cases. First, consider the case where the faces are on the Front and East boundaries. On the East face, the boundary conditions give the stresses t_{1e}, t_{5e}, and t_{6e}. These appear in (49)–(51) for the displacements averaged over the East face: u_{E}, v_{E}, and w_{E}. On the Front face, the boundary conditions give the stresses t_{3f}, t_{4f}, and t_{5f}. These appear in (171)–(173) for the displacements averaged over the Front face: u_{F}, v_{F}, and w_{F}. Four of these six equations require values for u_{FE} and w_{FE}. These values are approximated by extrapolation:

$$u_{\mathrm{FE}} = u_{\mathrm{E}} + \frac{\delta_{\mathrm{ZEFE}}}{\delta_{\mathrm{ZERE}}}(u_{\mathrm{E}} - u_{\mathrm{RE}}) \tag{177}$$

$$w_{\mathrm{FE}} = w_{\mathrm{F}} + \frac{\delta_{\mathrm{XFEF}}}{\delta_{\mathrm{XFWF}}}(w_{\mathrm{F}} - w_{\mathrm{FW}}). \tag{178}$$

The equations for the East face (49)–(51) depended on a two-sided approximation (52) for $\partial w/\partial z$. This two-sidedness introduced the need for w_{FE}. One could have approximated the derivative using a one-sided approximation based on w_{E} and w_{RE}; the two approximations would have the same order of accuracy. However, the ODEs for u_{P}, v_{P}, and w_{P} for this cell are equations (37)–(39) which also require values like w_{FE}. In principle, one could avoid this need by doing different approximations (resulting in different ODEs) for the boundary volumes. However, ex-

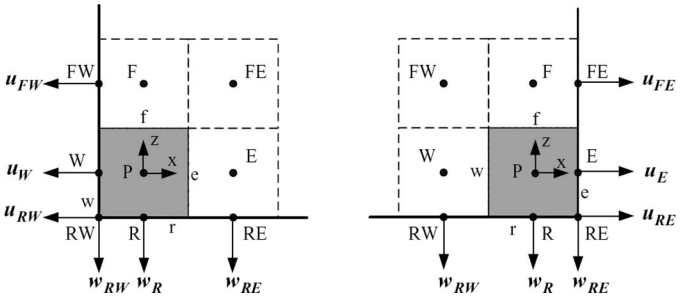

Fig. 20. Control volumes placed at the Rear-West and Rear-East boundaries.

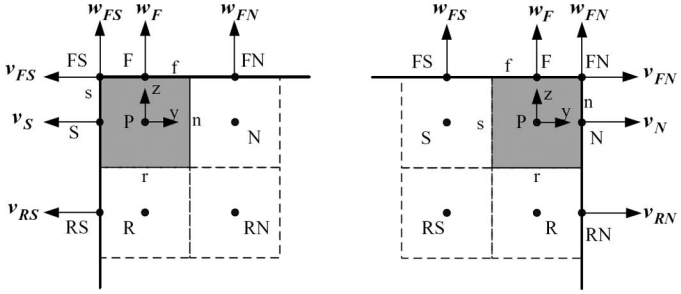

Fig. 21. Control volumes placed at the Front-South and Front-North boundaries.

trapolation allows one to avoid this, leading to a simpler program.

If the control volume has faces on the Front and West boundaries, the six boundary conditions enter into (162)–(164) and (171)–(173). Some of these equations require values for u_{FW} and w_{FW} which are approximated by extrapolation:

$$u_{\mathrm{FW}} = u_{\mathrm{W}} + \frac{\delta_{\mathrm{ZWFW}}}{\delta_{\mathrm{ZWRW}}}(u_{\mathrm{W}} - u_{\mathrm{RW}}) \tag{179}$$

$$w_{\mathrm{FW}} = w_{\mathrm{F}} + \frac{\delta_{\mathrm{XFWF}}}{\delta_{\mathrm{XFEF}}}(w_{\mathrm{F}} - w_{\mathrm{FE}}). \tag{180}$$

C. Edge Volume With Faces on the Rear and West Boundaries or the Rear and East Boundaries

Refer to Fig. 20 for the location of the control volume in these two cases. First, if the faces are on the Rear and West boundaries then three of the boundary conditions will enter into (162)–(164) for u_{W}, v_{W}, and w_{W} and three boundary conditions will enter into (174)–(176) for u_{R}, v_{R}, and w_{R}. These equations require u_{RW} and w_{RW} which are found by extrapolation:

$$u_{\mathrm{RW}} = u_{\mathrm{W}} + \frac{\delta_{\mathrm{ZWRW}}}{\delta_{\mathrm{ZWFW}}}(u_{\mathrm{W}} - u_{\mathrm{FW}}) \tag{181}$$

$$w_{\mathrm{RW}} = w_{\mathrm{R}} + \frac{\delta_{\mathrm{XRWR}}}{\delta_{\mathrm{XRER}}}(w_{\mathrm{R}} - w_{\mathrm{RE}}). \tag{182}$$

If the faces are on the Rear and East boundaries, then (49)–(51) and (174)–(176) are used, requiring u_{RE} and w_{RE}:

$$u_{\mathrm{RE}} = u_{\mathrm{E}} + \frac{\delta_{\mathrm{ZERE}}}{\delta_{\mathrm{ZEFE}}}(u_{\mathrm{E}} - u_{\mathrm{FE}}) \tag{183}$$

$$w_{\mathrm{RE}} = w_{\mathrm{R}} + \frac{\delta_{\mathrm{XRER}}}{\delta_{\mathrm{XRWR}}}(w_{\mathrm{R}} - w_{\mathrm{RW}}). \tag{184}$$

D. Edge Volume With Faces on the Front and South Boundaries or the Front and North Boundaries

Refer to Fig. 21 for the location of the control volume in these two cases. In the Front-South case, one uses (168)–(170) and (171)–(173). These require v_{FS} and w_{FS}:

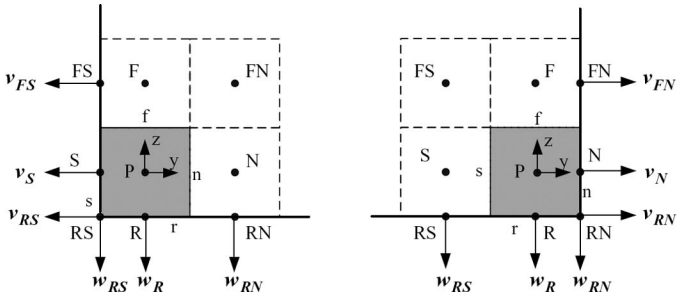

Fig. 22. Control volumes placed at the Rear-South and Rear-North boundaries.

$$v_{\mathrm{FS}} = v_{\mathrm{S}} + \frac{\delta_{\mathrm{ZSFS}}}{\delta_{\mathrm{ZSRS}}}(v_{\mathrm{S}} - v_{\mathrm{RS}}) \tag{185}$$

$$w_{\mathrm{FS}} = w_{\mathrm{F}} + \frac{\delta_{\mathrm{YFSF}}}{\delta_{\mathrm{YFNF}}}(w_{\mathrm{F}} - w_{\mathrm{FN}}). \tag{186}$$

In the Front-North case, one uses (165)–(167) and (171)–(173). These require v_{FN} and w_{FN}:

$$v_{\mathrm{FN}} = v_{\mathrm{N}} + \frac{\delta_{\mathrm{ZNFN}}}{\delta_{\mathrm{ZNRN}}}(v_{\mathrm{N}} - v_{\mathrm{RN}}) \tag{187}$$

$$w_{\mathrm{FN}} = w_{\mathrm{F}} + \frac{\delta_{\mathrm{YFNF}}}{\delta_{\mathrm{YFSF}}}(w_{\mathrm{F}} - w_{\mathrm{FS}}). \tag{188}$$

E. Edge Volume With Faces on the Rear and South Boundaries or the Rear and North Boundaries

Refer to Fig. 22 for the location of the control volume in these two cases. In the Rear-South case, one uses (168)–(170) and (174)–(176). These require v_{RS} and w_{RS}:

$$v_{\mathrm{RS}} = v_{\mathrm{S}} + \frac{\delta_{\mathrm{ZSRS}}}{\delta_{\mathrm{ZSFS}}}(v_{\mathrm{S}} - v_{\mathrm{FS}}) \tag{189}$$

$$w_{\mathrm{RS}} = w_{\mathrm{R}} + \frac{\delta_{\mathrm{YRSR}}}{\delta_{\mathrm{YRNR}}}(w_{\mathrm{R}} - w_{\mathrm{RN}}). \tag{190}$$

In the Rear-North case, one uses (165)–(167) and (174)–(176). These require v_{RN} and w_{RN}:

$$v_{\mathrm{RN}} = v_{\mathrm{N}} + \frac{\delta_{\mathrm{ZNRN}}}{\delta_{\mathrm{ZNFN}}}(v_{\mathrm{N}} - v_{\mathrm{FN}}) \tag{191}$$

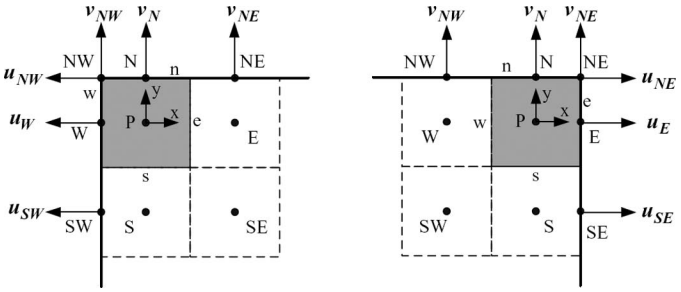

Fig. 23. Control volumes placed at the North-West and North-East boundaries.

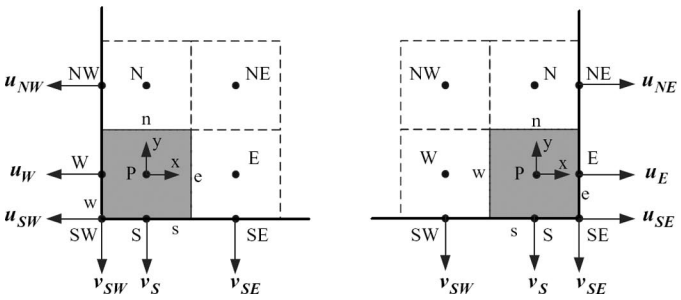

Fig. 24. Control volumes placed at the South-West and South-East boundaries.

$$w_{\mathrm{RN}} = w_{\mathrm{R}} + \frac{\delta_{\mathrm{YRNR}}}{\delta_{\mathrm{YRSR}}}(w_{\mathrm{R}} - w_{\mathrm{RS}}). \tag{192}$$

F. Edge Volume With Faces on the North and West Boundaries or the North and East Boundaries

Refer to Fig. 23 for the location of the control volume in these two cases. In the North-West case, one uses (162)–(164) and (165)–(167). These require u_{NW} and v_{NW}:

$$u_{\mathrm{NW}} = u_{\mathrm{W}} + \frac{\delta_{\mathrm{YWNW}}}{\delta_{\mathrm{YWSW}}}(u_{\mathrm{W}} - u_{\mathrm{SW}}) \tag{193}$$

$$v_{\mathrm{NW}} = v_{\mathrm{N}} + \frac{\delta_{\mathrm{XNWN}}}{\delta_{\mathrm{XNEN}}}(v_{\mathrm{N}} - v_{\mathrm{NE}}). \tag{194}$$

In the North-East case, one uses (49)–(51) and (165)–(167). These require u_{NE} and v_{NE}:

$$u_{\mathrm{NE}} = u_{\mathrm{E}} + \frac{\delta_{\mathrm{YENE}}}{\delta_{\mathrm{YESE}}}(u_{\mathrm{E}} - u_{\mathrm{SE}}) \tag{195}$$

$$v_{\mathrm{NE}} = v_{\mathrm{N}} + \frac{\delta_{\mathrm{XNEN}}}{\delta_{\mathrm{XNWN}}}(v_{\mathrm{N}} - v_{\mathrm{NW}}). \tag{196}$$

G. Edge Volume With Faces on the South and West Boundaries or the South and East Boundaries

Refer to Fig. 24 for the location of the control volume in these two cases. In the South-West case, one uses (162)–(164) and (168)–(170). These require u_{SW} and v_{SW}:

$$u_{\mathrm{SW}} = u_{\mathrm{W}} + \frac{\delta_{\mathrm{YWSW}}}{\delta_{\mathrm{YWNW}}}(u_{\mathrm{W}} - u_{\mathrm{NW}}) \tag{197}$$

$$v_{\mathrm{SW}} = v_{\mathrm{S}} + \frac{\delta_{\mathrm{XSWS}}}{\delta_{\mathrm{XSES}}}(v_{\mathrm{S}} - v_{\mathrm{SE}}). \tag{198}$$

In the South-East case, one uses (49)–(51) and (168)–(170). These require u_{SE} and v_{SE}:

$$u_{\mathrm{SE}} = u_{\mathrm{E}} + \frac{\delta_{\mathrm{YESE}}}{\delta_{\mathrm{YENE}}}(u_{\mathrm{E}} - u_{\mathrm{NE}}) \tag{199}$$

$$v_{\mathrm{SE}} = v_{\mathrm{S}} + \frac{\delta_{\mathrm{XSES}}}{\delta_{\mathrm{XSWS}}}(v_{\mathrm{S}} - v_{\mathrm{SW}}). \tag{200}$$

H. Control Volumes at Corners

Consider a control volume which has three faces in common with the boundary of the piezoelectric material. For each face, three stresses are specified. These enter into three equations, chosen from E: (49)–(51), W: (162)–(164), N: (165)–(167), S: (168)–(170), F: (171)–(173), and R: (174)–(176). This results in nine equations for nine unknowns. Extrapolations are done to approximate u, v, and w at the mid-points of the edges, to close the system of equations, similar to equations (177)–(200).

References

[1] R. Lerch, "Simulation of piezoelectric devices by 2-dimensional and 3-dimensional finite elements," *IEEE Trans. Ultrason. Ferroelectr. Freq. Control*, vol. 37, no. 3, pp. 233–247, 1990.

[2] H. Allik and T. J. R. Hughes, "Finite element method for piezoelectric vibration," *Int. J. Numer. Methods Eng.*, vol. 2, no. 2, pp. 151–157, 1970.

[3] J. Wang, J. d. Yu, Y.-K. Yong, and T. Imai, "A new theory for electroded piezoelectric plates and its finite element application for the forced vibrations of quartz crystal resonators," *Int. J. Solids Struct.*, vol. 37, no. 40, pp. 5653–5673, 2000.

[4] Y. Kagawa and T. Yamabuchi, "Finite element approach for a piezoelectric circular rod," *IEEE Trans. Sonics Ultrason.*, vol. SU-23, no. 10, pp. 370–385, 1976.

[5] Y. Kagawa and T. Yamabuchi, "Finite element simulation of a composite piezoelectric ultrasonic transducer," *IEEE Trans. Sonics Ultrason.*, vol. SU-26, no. 2, pp. 81–88, 1979.

[6] Y. Kagawa, T. Tsuchiya, T. Kataoka, T. Yamabuchi, and T. Furukawa, "Finite element simulation of dynamic responses of piezoelectric actuators," *J. Sound Vibrat.*, vol. 191, no. 4, pp. 519–538, 1996.

[7] N. W. Hagood and A. J. McFarland, "Modeling of a piezoelectric rotary ultrasonic motor," *IEEE Trans. Ultrason. Ferroelectr. Freq. Control*, vol. 42, no. 2, pp. 210–224, 1995.

[8] V. Bolborici, "Modeling of the stator of piezoelectric traveling wave rotary ultrasonic motors," Ph.D. dissertation, Dept. of Electrical and Computer Engineering, University of Toronto, Toronto, ON, Canada, 2009.

[9] R. D. Mindlin, "High frequency vibrations of piezoelectric crystal plates," *Int. J. Solids Struct.*, vol. 8, no. 7, pp. 895–906, 1972.

[10] N. E. Ghouti, "Hybrid modeling of traveling wave piezoelectric motor," Ph.D. dissertation, Dept. of Control Engineering, Aalborg University, Aalborg, Denmark, 2000.

[11] F. Giraud, "Modelisation causale et commende d'un actionneur piezo-electrique a onde progessive," Ph.D. dissertation, Laboratoire d'Electrotechnique et d'Electronique de Puissance, University of Lille, Lille, France, 2002.

[12] E. M. Syed, "Analysis and modeling of piezoelectric transformers," Master's thesis, Dept. of Electrical and Computer Engineering, University of Toronto, Toronto, ON, Canada, 2001.

[13] P. Pulpan, J. Erhart, and O. Stipek, "Analytical modeling of piezoelectric transformers," *Ferroelectrics*, vol. 351, pp. 204–215, 2007.

[14] C. Nadal and F. Pigache, "Multimodal electromechanical model of piezoelectric transformers by Hamiltons principle," *IEEE Trans. Ultrason. Ferroelectr. Freq. Control*, vol. 56, no. 11, pp. 2530–2543, 2009.
[15] D. Campolo, R. Sahai, and R. S. Fearing, "Development of piezoelectric bending actuators with embedded piezoelectric sensors for micromechanical flapping mechanisms," in *Proc. 2003 IEEE Int. Conf. Robotics and Automation*, 2003, pp. 3339–3346.
[16] E. V. Ardelean, D. G. Cole, and R. L. Clark, "High performance V-stack piezoelectric actuator," *J. Intell. Mater. Syst. Struct.*, vol. 15, no. 11, pp. 879–889, 2004.
[17] D. C. Lee, D. W. Yun, and C. S. Han, "A material rigidity effect of a bimorph piezoelectric actuator," *Smart Mater. Struct.*, vol. 16, no. 4, pp. 1043–1049, 2007.
[18] H. K. Versteeg and W. Malalasekera, *An Introduction to Computational Fluid Dynamics. The Finite Volume Method*. New York, NY: Pearson Education Ltd., 2007.
[19] R. J. LeVeque, *Finite-Volume Methods for Hyperbolic Problems*. New York, NY: Cambridge University Press, 2002.
[20] H. S. Tzou, *Piezoelectric Shells Distributed Sensing and Control of Continua*. Boston, MA: Kluwer Academic Publishers, 1993.
[21] J. T. Hsu and L. Vu-Quoc, "A rational formulation of thermal circuit models for electrothermal simulation—Part 1: Finite element method," *IEEE Trans. Circuits Syst. I*, vol. 43, no. 9, pp. 721–732, 1996.
[22] A. S. Ekinci and A. Atalar, "An electrical circuit theoretical method for time- and frequency- domain solutions of the structural mechanics problems," *Int. J. Numer. Methods Eng.*, vol. 45, no. 10, pp. 1485–1507, 1999.
[23] T. E. McDermott, P. Zhou, and J. Gilmore, "Electromechanical system simulation with models generated from finite element solutions," *IEEE Trans. Magn.*, vol. 33, no. 2, pp. 1682–1685, 1997.

Valentin Bolborici was born in Romania in 1968. He received his B.S. degree in electrical engineering from the University of Craiova in 1992 and his M.A.Sc. and Ph.D. degrees in electrical engineering from the University of Toronto in 1999 and 2009, respectively. He is currently enrolled in a post-doctoral program at the University of Toronto. From 1995 to 1998, he worked as a test engineer for American Sensors Inc., Toronto. After completing his Master's degree, he worked as an electrical engineer in the aerospace industry at MD Robotics in Canada from 2000 and 2002, and as a senior electrical engineer in the electrical power drive industry at Hitachi Ltd. in Japan from 2002 to 2003. His research interests include modeling and control of piezoelectric devices, optimization of high frequency magnetic components, microprocessor controlled electric drives, and modeling of hybrid energy storage systems.

Francis Dawson (S'86–M'87) received the B.Sc degree in physics and the B.ASc., M.A.Sc., and Ph.D degrees in electrical engineering from the University of Toronto in 1978, 1982, 1985, and 1988, respectively.

He worked as a process control engineer in the pulp and paper, rubber, and textile industries during the period from 1978 to 1980. From 1982 to 1984, he acted as a consultant on various projects. Development areas included high-frequency link power supplies, power supplies for specialized applications, and high-current protection circuits. Since 1988, he has been with the Department of Electrical and Computer Engineering, University of Toronto, where he is engaged in teaching and research.

His areas of research interest include static power converters and their applications, signal processing in power engineering applications, energy storage systems, and device or process modeling. He has also participated as a Consultant or Project Leader in several industrial projects. Dr. Dawson is a member of the Association of Professional Engineers of Ontario and is an IEEE Fellow.

Mary Pugh was born in Washington, DC, in 1966. She received a B.A. degree in pure mathematics from U.C. Berkeley in 1986, and the M.S. and Ph.D. degrees in mathematics from the University of Chicago in 1988 and 1993, respectively. From 1993 to 1997, she was a post-doc at the Courant Institute and at the Institute for Advanced Study. From 1997 to 2001, she was an assistant professor at The University of Pennsylvania. Since 2001, she has been an associate professor at the University of Toronto. Her research is largely on the modeling, analysis, and simulation of thin films of viscous liquids, with a broader interest in computational methods for partial differential equations.